Transit-Time and Tracer-Age Distributions in Geophysical Flows

MARK HOLZER

Canadian Centre for Climate Modelling and Analysis, Atmospheric Environment Service, University of Victoria, Victoria, British Columbia, Canada

TIMOTHY M. HALL

NASA Goddard Institute for Space Studies and Columbia University, New York, New York

(Manuscript received 4 January 1999, in final form 2 August 1999)

ABSTRACT

Transport in the atmosphere and in the ocean is the result of the complex action of time-dependent and often highly turbulent flow. A useful diagnostic that summarizes the rate at which fluid elements are transported from some region to a point (or the reverse) via a multiplicity of pathways and mechanisms is the probability density function (pdf) of transit times. The first moment of this pdf, often referred to as ''mean age,'' has become an important transport diagnostic commonly used by the observational community.

This paper explores how to probe the flow with passive tracers to extract transit-time pdf's. As a foundation, the literal ''tracer age'' is defined as the elapsed time since tracer was injected into the flow, and the corresponding tracer-age distribution, Z, as the fractional tracer mass in a given interval of tracer age. The distribution, Z, has concrete physical interpretation for arbitrary sources, but is only equivalent to a tracer-independent transit-time pdf of the flow in special cases. The transit-time pdf is a propagator, $\mathcal{G}'$, of boundary conditions (the ''age spectrum'' of T. M. Hall and R. A. Plumb) applied over a control surface, Ω. The propagator $\mathcal{G}'$ is shown to be the flux into Ω resulting from a unit mass injected into the time-reversed flow. Through explicit construction of the transit-time pdf using the concept of tracer age, the special cases for which Z and $\mathcal{G}'$ coincide are established. This allows a direct physical demonstration of $\mathcal{G}'$, and its adjoint $\mathcal{G}'^{\dagger}$, as the pdf's of transit times since fluid at point $\mathbf{r}$ had last contact with Ω, and until fluid at $\mathbf{r}$ will have first contact with Ω, respectively. In the limit as Ω is shrunk to a point, point-to-point transit-time pdf's are well defined, but their mean transit time and higher-order moments become infinite. Several concrete geophysical examples are considered to illustrate under what conditions characteristics of tracer-age and transit-time pdf's can be inferred from observations in the atmosphere or the ocean.

1. Introduction

Trace gases are an important part of the atmosphere not only because their radiative and chemical properties affect climate but also because they directly probe atmospheric transport. Routine observations of winds do not sample the atmosphere sufficiently to resolve many mechanisms important for global transport, such as convection, tropopause folds, breaking gravity waves, and boundary-layer mixing. Measurements of tracers provide one of the best ways to quantify transport rates and to assess the realism of transport in atmospheric models. To this end, considerable effort continues to be expended on measurements of chemically long-lived tracers from ground-based stations, aircraft, balloon, and satellite platforms (e.g., Bischof et al. 1985; Luo et al. 1994; Maiss et al. 1996; Boering et al. 1996; Geller et al. 1997; Elkins et al. 1996; Mote et al. 1998). However, direct and unambiguous determination of transport properties from tracer data is often difficult or impossible because the sources and sinks of tracers are imperfectly known. Even assuming perfect knowledge of sources and sinks, transport information is intricately entangled with their spatial and temporal variability. Therefore, a diagnostic framework connecting tracer distributions to tracer-independent transport properties of the flow is a valuable tool for the interpretation of observations.

One component of such a framework is what Hall and Plumb (1994, hereafter HP94) called the ''age spectrum.'' The age spectrum, $\mathcal{G}'$, is a diagnostic of the flow independent of the distribution of any tracer and summarizes the rate at which fluid is transported from a region Ω to a point $\mathbf{r}$. More precisely, $\mathcal{G}'$, is the probability density function (pdf) of Ω-to-$\mathbf{r}$ transit times. In this paper, we therefore refer to the age spectrum as the

Corresponding author address: Dr. Mark Holzer, Canadian Centre for Climate Modelling and Analysis, Atmospheric Environment Service, University of Victoria, Victoria, BC V8W 2Y2, Canada.
E-mail: mark.holzer@ec.gc.ca

transit-time pdf and reserve ''tracer-age distribution'' for a distinct quantity defined below. The pdf $\mathcal{G}'$ is typically broadly distributed, reflecting the multiplicity of Ω-to-**r** pathways available to the fluid. Transit-time pdf's have been discussed and applied to stratospheric transport analysis by Kida (1983) and by HP94. HP94 defined the age spectrum as the distribution of times since the fluid elements constituting a given stratospheric air parcel had last contact with the troposphere. The mean transit time, Γ, at a point in the stratosphere (''mean age'' in the language of HP94) is the average time since the air there was last in the troposphere. The transit-time pdf has proved to be a useful conceptual tool for interpreting tracer observations in the stratosphere. Although $\mathcal{G}'$ itself is not directly observable, Γ can be inferred from measurements of appropriate tracers (e.g., Elkins et al. 1996; Boering et al. 1996), and measurements of combinations of tracers can be used to constrain the shape of $\mathcal{G}'$ in the lower stratosphere (Andrews et al. 1999).

HP94 formulated the transit-time pdf in terms of boundary conditions on mixing ratio by analyzing the stratospheric response to a short-lived impulse in mixing ratio imposed near the earth's surface. This is a natural approach for the stratosphere, into which most air and tracer enters through the tropical tropopause regardless of its history or source–sink distribution in the troposphere. In many situations, however, it is more physical to consider tracer distributions as arising from specified sources and sinks rather than from imposed mixing ratios at the surface. For example, the distribution of CO_2 in the troposphere, including near the surface, is usually considered to be determined by the combination of atmospheric transport and surface sources and sinks, rather than transport and imposed surface mixing ratio.

In this paper we establish a novel conceptual and analytical framework that connects the transit-time pdf with a closely related, but generally distinct, distribution of tracer age. The tracer-age distribution, Z, keeps track of the time for which tracer particles have been in the flow, and is defined here as the fraction of current tracer mass binned according to the time (i.e., age) it has been in the flow. As we shall show, consideration of explicit sources and sinks rather than mixing ratio boundary conditions leads naturally to the tracer-age distribution, Z, and mean tracer age, A, which are complimentary to $\mathcal{G}'$ and Γ. Expressing Z and $\mathcal{G}'$ in terms of Green functions, we capitalize on powerful analytic relationships and derive the special circumstances under which Z and $\mathcal{G}'$ coincide, thereby confirming HP94's interpretation of $\mathcal{G}'$ as the pdf of times since an air parcel *last* had contact with a specified region, Ω. Our approach, however, is general and also includes the pdf of times for an air parcel to have *first* contact with Ω. We illustrate these concepts with examples from both simple analytic models and from numerical atmospheric transport models, and we demonstrate how characteristics of $\mathcal{G}'$ and Z can be inferred from real tracers. We also explore the dependence of the transit-time pdf on the size of Ω and find the general result for advecting-diffusing systems that mean transit times become infinite as Ω is shrunk to a point.

While the atmosphere provides the context and language for this paper, the development has more general applicability. Embedding the transit-time pdf in the general framework of Green functions provides a guide for synthesizing measurements of tracer into a coherent, physical picture of transport, without regard to the particular geophysical setting. Oceanographers commonly describe oceanic tracer transport in terms of ''age,'' generally construed as the mean time since a water parcel last had contact with the ocean surface (e.g., Jenkins 1987; England 1995), and Beining and Roether (1996) discuss age distributions for ocean parcels, a concept related to the pdf's developed here. Following examples for the atmosphere, we briefly discuss application of our approach to the ocean. Advecting-diffusing systems are in fact so common in nature that the applicability of these concepts extends to nongeophysical fields, such as migrating biological populations (e.g., Zabel and Anderson 1997), though we will address only geophysical issues here.

2. Green functions and boundary propagator

We now introduce Green functions for passive tracer transport and develop their connection to a propagator of boundary conditions (BCs) on mixing ratio, which has the interpretation of a transit-time pdf. Details of the general solution for mixing ratio in terms of Green functions are provided in appendix A. The development in this section is general, but throughout we provide illustrations from simple analytical models whose details are provided in appendixes B and C. In section 5 examples from more realistic general circulation models (GCMs) are given. Additional examples of Green functions in a GCM context may by found in Holzer (1999).

a. Green functions

The Green function is a natural analytical tool for the study of transport because the continuity equation for a passive tracer is linear in the mass mixing ratio, χ. We write the tracer continuity equation as

$$(\partial_t + \mathcal{T})\chi = S, \tag{1}$$

where the linear transport operator $\mathcal{T}$ represents advection and diffusion (and, in a model context, parameterized subgrid-scale processes such as convection), and S represents a specified source of tracer. Although formally it does not matter whether the diffusive part of $\mathcal{T}$ represents molecular diffusion or turbulent diffusion, for physical interpretations of our results we will assume throughout that any diffusion in $\mathcal{T}$ models the mixing due to small-scale turbulent advection and that molecular diffusion is negligible. The linearity of (1) allows

χ to be synthesized as a linear superposition of the mixing ratios from individual source pulses. We, therefore, consider S to be a collection of pulses localized in space and time, which in the limit become Dirac δ functions. Equation (1) with S being one such δ function defines the corresponding Green function, G, that is,

$$(\partial_t + \mathcal{T})G(\mathbf{r}, t|\mathbf{r}', t') = \rho^{-1}\delta(t - t')\delta^3(\mathbf{r} - \mathbf{r}'), \quad (2)$$

where ρ is the density of the fluid. Thus, G has dimensions of inverse mass and corresponds to tracer injected at the point $(\mathbf{r}', t')$ normalized by the mass injected. Because there cannot be any tracer in the fluid before it has been injected, G is said to satisfy the causality condition that $G = 0$ for $t' > t$. The solutions of (1) and (2) depend on a consistent set of BCs.

The solution of linear differential equations subject to arbitrary BCs and interior sources is derived in terms of the corresponding Green functions in great generality by Morse and Feshbach (1953, hereafter MF53), while Butkov (1968, chapter 12) provides a discussion more oriented toward simple examples. For the convenience of the reader, the general solution to (1) for general $\mathcal{T}$, and for the special case of generic advective-diffusive transport, is also presented in appendix A. We consider here only the familiar case of generic advection-diffusion, namely,

$$\mathcal{T}(\chi) = \mathbf{v}\cdot\boldsymbol{\nabla}\chi - \rho^{-1}\boldsymbol{\nabla}\cdot(\rho\kappa\boldsymbol{\nabla}\chi), \quad (3)$$

with advecting velocity, $\mathbf{v}(\mathbf{r}, t)$, and isotropic (eddy-) diffusivity, $\kappa(\mathbf{r}, t)$. (Generalization to anisotropic diffusivity is straightforward, but not considered explicitly here.) Denoting the Green function satisfying generic BCs by G_x, the general solution of (1) with (3) is (see appendix A)

$$\begin{aligned}\chi(\mathbf{r}, t) = &\int d^3r'\ \rho(\mathbf{r}', 0)G_x(\mathbf{r}, t|\mathbf{r}', 0)\chi(\mathbf{r}', 0)\\ &+ \int_0^t dt' \int d^3r'\rho(\mathbf{r}', t')G_x(\mathbf{r}, t|\mathbf{r}', t')S(\mathbf{r}', t')\\ &+ \int_0^t dt' \int_\partial d^2r_s\ \hat{\mathbf{n}}\cdot\mathbf{C}, \end{aligned} \quad (4)$$

where

$$\begin{aligned}\mathbf{C} \equiv\ &\rho(\mathbf{r}_s, t')\kappa(\mathbf{r}_s, t')[G_x(\mathbf{r}, t|\mathbf{r}_s, t')\boldsymbol{\nabla}\chi(\mathbf{r}_s, t')\\ &- \chi(\mathbf{r}_s, t')\boldsymbol{\nabla}G_x(\mathbf{r}, t|\mathbf{r}_s, t')]\\ &- \rho(\mathbf{r}_s, t')\mathbf{v}(\mathbf{r}_s, t')\chi(\mathbf{r}_s, t')G_x(\mathbf{r}, t|\mathbf{r}_s, t'), \end{aligned} \quad (5)$$

and the gradients are evaluated for $\mathbf{r}_s$ on the boundary, ∂, of the geophysical reservoir under consideration (e.g., the earth's surface for the atmosphere). The first term of (4) represents the time-evolved initial condition $\chi(\mathbf{r}', 0)$. The second term is the superposition of all the tracer pulses emitted at points $\mathbf{r}'$ and times t' by the source $S(\mathbf{r}', t')$. The last term is an integral over the boundary (outward normal $\hat{\mathbf{n}}$) and represents any contributions to χ due to the BCs imposed on χ and/or $\hat{\mathbf{n}}\cdot\boldsymbol{\nabla}\chi$. In addition, there may be an independently specified BC on the normal flow, $\hat{\mathbf{n}}\cdot\mathbf{v}$. We will consider only two specific sets of BCs, discussed next.

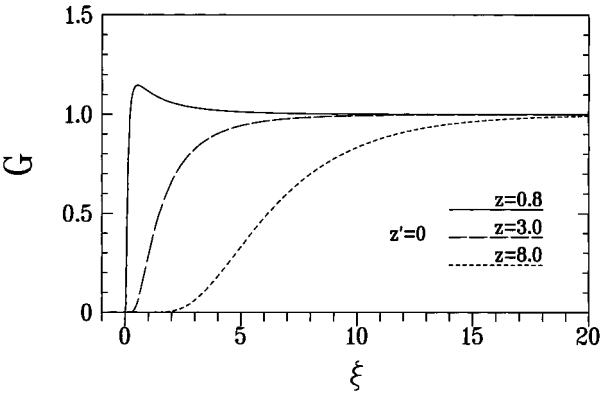

FIG. 1. Analytical solutions of $G(z, z', \xi)$ for the stationary 1D model atmosphere of appendix B, as a function of elapsed time, ξ. The source point z' is located at the "surface," $z' = 0$. The time evolution of G is plotted at the three locations, z, indicated. Note that with increasing time $G \to G_\infty = 1$, uniformly for all z.

1) Zero-flux boundary conditions

The first case of BCs considered is zero flux on all the boundaries of the geophysical reservoir, which also implies zero normal velocity at the boundaries. From here on we use a plain G to denote the Green function subject to zero-flux BCs. With these BCs, the boundary term of (4) vanishes entirely and the general solution to (1) becomes

$$\begin{aligned}\chi(\mathbf{r}, t) = &\int dm'\ G(\mathbf{r}, t|\mathbf{r}', 0)\chi(\mathbf{r}', 0)\\ &+ \int_0^t dt' \int dm'\ G(\mathbf{r}, t|\mathbf{r}', t')S(\mathbf{r}', t'), \end{aligned} \quad (6)$$

where $dm' \equiv \rho(\mathbf{r}', t')\, d^3r'$. Note that this case includes specified surface fluxes as these can be considered as interior sources or sinks placed arbitrarily close to the boundary. [Alternatively, $\hat{\mathbf{n}}\cdot\boldsymbol{\nabla}\chi$ could be specified as a flux BC, which would lead to an additional boundary contribution given by the first term of (5). However, for our purposes it is more convenient to regard specified surface fluxes as sources and use (6).]

Because zero-flux BCs are imposed on G, the tracer "mass," $\int dm\ G = 1$, is conserved. Ultimately, the initial unit tracer mass injected is uniformly spread over the entire reservoir so that G has the constant long-term, spatially uniform limit of G_∞, where $G_\infty = \int dm\ G / \int dm = 1/M_A$ is the inverse mass of the fluid (assumed constant).

Figure 1 shows G for the simple case of a one-dimensional (1D) diffusive atmosphere (exponentially decaying fluid density; for details see appendix B). Be-

cause this model's transport is stationary, G depends on time only through the elapsed time (or "lag time") $t - t' \equiv \xi$. For the G shown, the source is located at the bottom boundary ($z' = 0$). Note that for long times, G approaches a constant $G_\infty = 1$, and that G overshoots G_∞ at locations, z, close to the source. The overshoot is a generic feature of G (Holzer 1999).

We emphasize that closed-form analytical solutions for Green functions are rare exceptions and only possible for very simple cases. In the general case, G is physically a "puff" of time-evolving mixing ratio that typically becomes rapidly shredded and filamented by the time-evolving velocity field. The complicated dependence of G on the flow is manifest when expressing G as a (Feynman-type) path integral (see, e.g., Shraiman and Siggia 1994), though we will not make use of path integrals in this paper.

2) Boundary conditions on mixing ratio

The second set of BCs considered imposes a specified mixing ratio over a control surface Ω that is fixed in space. The surface Ω can be part of the physical boundary of the domain (e.g., a patch of the earth's surface) or an interior surface, depending on the application. Everywhere else on the boundary of the domain we impose zero-flux BCs. The appropriate homogeneous BCs to be imposed on the Green function are zero mixing ratio on Ω and zero flux elsewhere (see also MF53). We denote the Green function with these BCs by G_0, so that from (4)

$$\chi(\mathbf{r}, t) = \int dm'\, G_0(\mathbf{r}, t|\mathbf{r}', 0)\chi(\mathbf{r}', 0) + \int_0^t dt' \int dm'\, G_0(\mathbf{r}, t|\mathbf{r}', t')S(\mathbf{r}', t') - \int_0^t dt' \int_\Omega d^2r_s\, \rho(\mathbf{r}_s, t')\kappa(\mathbf{r}_s, t')\chi(\mathbf{r}_s, t') \hat{\mathbf{n}} \cdot \nabla_{r_s} G_0(\mathbf{r}, t|\mathbf{r}_s, t'), \quad (7)$$

where the subscript on ∇_{r_s} indicates that the gradient is evaluated at points $\mathbf{r}_s$ on Ω. The purely diffusive nature of the boundary term in (7) is general and simply due to the BC $G_0 = 0$ on Ω.

Because of the zero-mixing-ratio BCs on G_0 over Ω (denoted as χ0BC), G_0 leaks continuously out of Ω so that G_0 has the long-time limit of zero. Note that if the source point, $\mathbf{r}'$, lies on Ω, then $G_0(\mathbf{r}, t|\mathbf{r}', t') = 0$ at all points $\mathbf{r}$. This is a statement of the fact that as the source point approaches Ω, mass is lost at an increasing rate, until a source right on Ω looses all its mass instantaneously.

Figure 2 shows G_0 as a function of elapsed time, $t - t' \equiv \xi$, for the 1D atmosphere of appendix B. Zero-mixing-ratio BCs are imposed at the bottom boundary (i.e., Ω corresponds to $z = 0$). Note that $G_0 \to 0$ as $\xi \to \infty$ and that the evolution of G_0 depends on the proximity of the field point, z, to both the source point, z', and to Ω. The largest response, G_0, to the initial unit mass injection is seen at the source location. Close to Ω, the χ0BCs exert a stronger influence resulting in a smaller amplitude of G_0. The most slowly decaying response can be seen at the field point most remote from Ω.

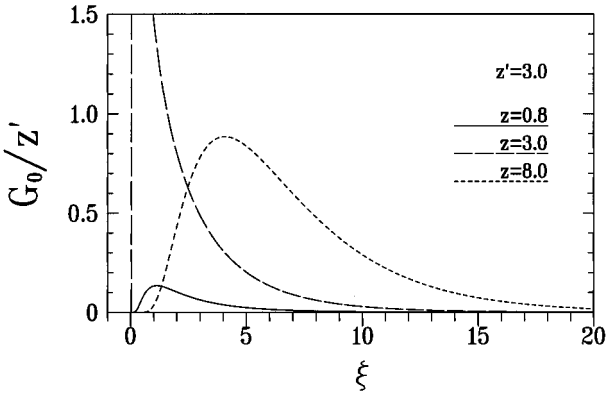

FIG. 2. Analytical solutions of $G_0(z, z', \xi)$ for the stationary 1D model atmosphere of appendix B, as a function of elapsed time, ξ. The source point is located at $z' = 3.0$. The zero-mixing-ratio BC is applied at the surface, $z = 0$. The time evolution of G_0 is plotted at the three locations, z, indicated.

b. Boundary propagator and transit-time pdf

We now define a boundary propagator, G', that makes use of the fact that a BC on mixing ratio specified on the surface, Ω, can be represented as a sum of δ functions in time and surface location. By contrast G and G_0 were based on a δ function decomposition of the sources. Thus, G' is directly defined through a δ function BC without any explicit sources, that is, G' satisfies

$$(\partial_t + \mathcal{T})G'(\mathbf{r}, t|\mathbf{r}_0, t') = 0, \quad (8)$$

subject to the BC

$$G'(\mathbf{r}_s, t|\mathbf{r}_0, t') = \delta(t - t')\delta^2(\mathbf{r}_s - \mathbf{r}_0), \quad (9)$$

where $\mathbf{r}_s$ and $\mathbf{r}_0$ are points on Ω. The solution to (1) resulting from the general BC, $\chi(\mathbf{r}_0, t)$, in the absence of explicit sources, is then given by

$$\chi(\mathbf{r}, t) = \int dt' \int_\Omega d^2r_0\, G'(\mathbf{r}, t|\mathbf{r}_0, t')\chi(\mathbf{r}_0, t'), \quad (10)$$

as can be verified by direct substitution. Hence G' "propagates" the BC on χ from Ω into the interior of the domain. Note that causality demands here that $G'(\mathbf{r}, t|\mathbf{r}_0, t') = 0$ for $t' > t$.

The normalization of G' follows from (10). Consider the case $\chi(\mathbf{r}_0, t) = \Theta(t - t_0)$, where the Heaviside function $\Theta(t - t_0)$ is unity for $t > t_0$ and zero otherwise. In that case, after waiting for an infinitely long time ($t_0 \to -\infty$), the boundary value of unity will have propagated throughout the domain, and if the domain is finite

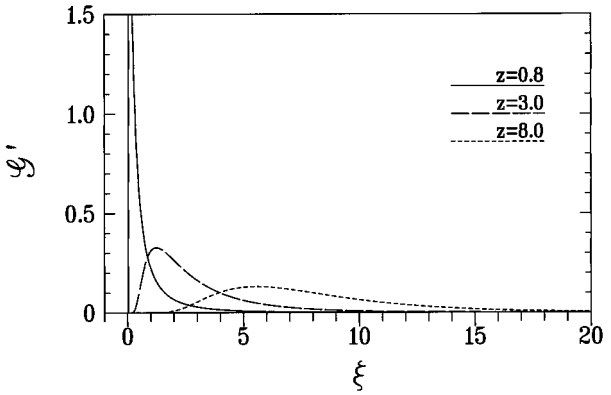

FIG. 3. Analytical solutions for the boundary propagator $\mathcal{G}'(z, \xi)$ for the stationary 1D model atmosphere of appendix B, as a function of elapsed time, ξ. The zero-mixing-ratio BC is applied at the surface, $z = 0$. The time evolution of $\mathcal{G}'$ is plotted at the three locations, z, indicated.

(as is any reasonable geophysical reservoir) then $\chi(\mathbf{r}, t) = 1$, giving the normalization

$$\int_{-\infty}^{t} dt' \int_{\Omega} d^2 r_0 \, G'(\mathbf{r}, t | \mathbf{r}_0, t') = 1. \qquad (11)$$

[For infinite domains, the right-hand side of (11) can vary spatially—see appendix Ca.] Based on (11), the surface integral

$$\mathcal{G}'(\mathbf{r}, t | \Omega, t') \equiv \int_{\Omega} d^2 r_0 \, G'(\mathbf{r}, t | \mathbf{r}_0, t'), \qquad (12)$$

is interpreted by HP94 as an ''age spectrum,'' that is, a pdf of Ω-to-$\mathbf{r}$ transit times. (Note that HP94 use the symbol G for the age spectrum.) As we will show below, $dt' \; \mathcal{G}'(\mathbf{r}, t | \Omega, t')$ is the probability that a fluid element at $(\mathbf{r}, t)$ had last contact with Ω at a time between $\xi \equiv t - t'$ and $\xi + d\xi$ ago.

Note that a propagator, G', for general BCs on mixing ratio over an extended surface, Ω, such as the earth's surface, must be defined as in (8) and (9). Boundary propagators with the $\delta(t - t')$ BC applied only to a small subregion of Ω, and zero-flux BCs elsewhere on Ω, cannot be used to synthesize the response to an Ω-distributed BC on mixing ratio from a superposition of such propagators. The G' only combine appropriately via (10) when the BC (9) applies over the entire control surface, Ω.

Figure 3 illustrates the general character of $\mathcal{G}'$ as a function of elapsed time $t - t' \equiv \xi$ for the 1D atmosphere of appendix B. Close to Ω (in this case, $z = 0$), most fluid elements have experienced a short transit time since they were last at Ω, and $\mathcal{G}'$ is sharply peaked. With increasing distance, z, from Ω the most probable time since last contact with Ω (where $\mathcal{G}'$ is peaked), moves to progressively longer times, and $\mathcal{G}'$ becomes increasingly broad, indicating an increasing multiplicity of possible transit times since last contact with Ω (see also HP94).

c. Probabilistic interpretations

For a physical and probabilistic interpretation of the Green functions it is useful to have a concept of the entity that is being transported. To this end, we envision the fluid as consisting of the standard ''material fluid elements'' of fluid mechanics. A subtlety arises when we consider a tracer. Generally tracer molecules that label a material fluid element do not remain confined to that fluid element but rather diffuse to adjacent fluid elements by molecular diffusion. However, we are interested here in the limiting case where the molecular diffusivity is negligible compared to the turbulent diffusivity (large Péclet number). Therefore, we regard any diffusion in the transport operator, $\mathcal{T}$, as modeling the effect of small-scale turbulent advection, so that diffusion is a characteristic of the flow and not of the material properties of the fluid-tracer combination. The turbulent diffusion of $\mathcal{T}$ transports fluid elements, or simply ''particles,'' and tracer is simply the substance that labels (''marks'') these particles. The mixing ratio at any point can be imagined as the marked mass fraction of a large number of particles constituting a ''fluid parcel.'' A parcel is imagined to have finite but arbitrarily small volume in the continuum limit.

The Green functions G and G_0 have the probabilistic interpretation of being pdf's so that $G \, dm$ is the probability of finding a tracer-marked particle in the fluid mass element dm at time t, if that particle was located at $\mathbf{r}'$ at time t', and similarly for G_0. Correspondingly, the domain-integrated masses, $M \equiv \int dm \; G = 1$ and $M_0(t | \mathbf{r}', t') \equiv \int dm \; G_0(\mathbf{r}, t | \mathbf{r}', t')$, have the interpretation of being the probabilities that a marked particle released at $(\mathbf{r}', t')$ is still marked a time $t - t'$ later. In the case of G (zero-flux BCs), once the particle has been marked with tracer, it will remain marked forever and is, therefore, to be found somewhere with unit probability. In the case of G_0 (zero-mixing-ratio BCs), the marked particle will eventually make contact with the $\chi 0$BC control surface, where it will loose its tracer marker, so that M_0 approaches zero for long $t - t'$. The decaying probability M_0 is shown in Fig. 4 for the 1D atmosphere of appendix B with Ω being the ''surface'' $z = 0$. Note that the closer the source point, z', is to Ω, the faster M_0 leaks out of the atmosphere.

The ''pseudo mass'' $M'(t | \mathbf{r}_0, t') \equiv \int dm \, G'(\mathbf{r}, t | \mathbf{r}_0, t')$ is not dimensionless and hence not a probability. However, for total fluid mass $M_A = \int dm$, the ratio $P(t | t') \equiv \int_{\Omega} d^2 r_0 \, M'/M_A = \int dm \; \mathcal{G}'/M_A$ can be interpreted as a pdf. [Note that $\int_0^{\infty} d\xi \, P(t | t - \xi) = 1$.] We may think of $P(t | t')$ as the pdf of ''population particle age,'' $\xi \equiv t - t'$, for surface-marked particles which are ''born'' on Ω and ''die'' when they make contact with Ω a second time. To see this, rewrite $P(t | t')$ as $\int d^3 r \; \mu(\mathbf{r}, t) \mathcal{G}'(\mathbf{r}, t | \Omega, t')$, where $\mu(\mathbf{r}, t) \equiv \rho(\mathbf{r}, t)/M_A$ is the pdf of finding a particle

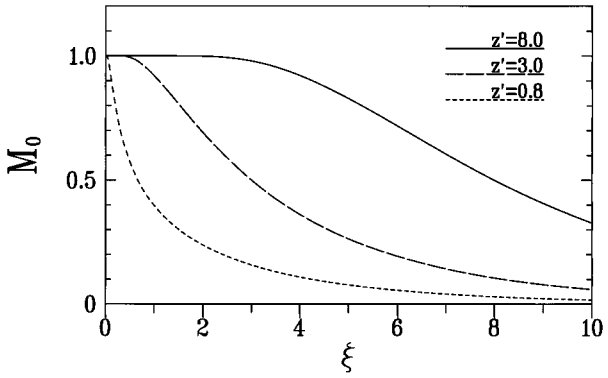

FIG. 4. The probability $M_0(z', \xi)$ in the analytical 1D atmosphere of appendix B, that a marked fluid particle located at z' at time $\xi = 0$ will not have made contact with the surface, $z = 0$, a time ξ later. As expected, the farther z' is from the surface, the longer it takes until the particle has significant probability of surface contact.

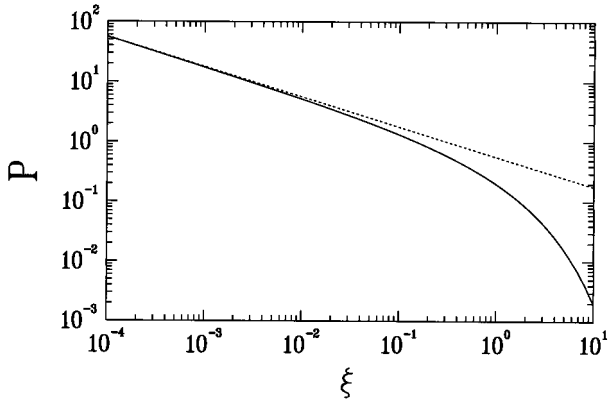

FIG. 5. The particle-age pdf, $P(\xi)$, of the 1D atmosphere of appendix B. Note the $\xi^{-1/2}$ divergence as $\xi \to 0$. (The dotted line indicates the asymptotic $\xi^{-1/2}$ power law.) This divergence is a generic feature of transport with a diffusive component and not a peculiarity of the 1D model (see section 2d).

in the volume d^3r. Given HP94's interpretation of $\mathcal{G}'$ as the pdf of times since last Ω contact, the product $\mu(\mathbf{r}, t)\mathcal{G}'(\mathbf{r}, t\,|\,\Omega, t')$ is the (joint) probability density for finding a particle in the volume d^3r that had last surface contact in the interval $(t', t' + dt')$, and hence has particle age in the interval $(\xi, \xi + d\xi)$. Integrating this joint probability density over $\mathbf{r}$, gives the pdf, $P(t\,|\,t')$, for finding in the entire population of particles a particle whose age lies in the interval $(\xi, \xi + d\xi)$. In the following subsection, we confirm HP94's interpretation of $\mathcal{G}'$ from a new approach and show that $P(t\,|\,t')$ is singular at $t = t'$ for advective-diffusive transport. Figure 5 shows the pdf, P, as a function of particle age, $t - t' \equiv \xi$, for the 1D atmosphere of appendix B. The pdf P diverges like $\xi^{-1/2}$ as $\xi \to 0$ for this model as indicated on the figure.

d. G′ as flux of G_0 in the time-reversed flow

From the general solution (7) for arbitrary BC's on mixing ratio, we can obtain an expression relating G' to G_0, which provides important new insight into the interpretation of G'. The boundary propagator G' is the special case of a δ-function BC on Ω, zero initial conditions, and no explicit sources. Substituting $\chi(\mathbf{r}_s, t') = \delta(t' - t_0)\delta^2(\mathbf{r}_s - \mathbf{r}_0)$ into (7) immediately gives

$$G'(\mathbf{r}, t\,|\,\mathbf{r}_0, t_0) = -\rho(\mathbf{r}_0, t_0)\kappa(\mathbf{r}_0, t_0)[\hat{\mathbf{n}} \cdot \boldsymbol{\nabla}_{\mathbf{r}'} G_0^\dagger(\mathbf{r}', t_0\,|\,\mathbf{r}, t)]_{\mathbf{r}'=\mathbf{r}_0}, \quad (13)$$

where we have expressed G_0 in terms of its adjoint $G_0^\dagger$, which is related to G_0 via the reciprocity condition $G_0(\mathbf{r}, t\,|\,\mathbf{r}', t') = G_0^\dagger(\mathbf{r}', t'\,|\,\mathbf{r}, t)$ (see, e.g., MF53). Causality for $G_0^\dagger(\mathbf{r}', t'\,|\,\mathbf{r}, t)$ demands that $t \geq t'$, as it does for $G_0(\mathbf{r}, t\,|\,\mathbf{r}', t')$. The reciprocity condition is the crucial ingredient in obtaining a general physical interpretation for G'. While $G(\mathbf{r}, t\,|\,\mathbf{r}', t')$ takes tracer from $(\mathbf{r}', t')$ to $(\mathbf{r}, t)$ in the flow evolving forward in time, $G^\dagger(\mathbf{r}', t'\,|\,\mathbf{r}, t)$ takes tracer from $(\mathbf{r}, t)$ to $(\mathbf{r}', t')$ in the time-reversed flow, whose transport operator is $\mathcal{T}^\dagger$. Thus, $G'(\mathbf{r}, t\,|\,\mathbf{r}_0, t_0)$ has the interpretation of the flux through the control surface, Ω, at $(\mathbf{r}_0, t_0)$ resulting from a unit-mass injection into the time-reversed flow at $(\mathbf{r}, t)$.

It is worth pointing out precisely what "time-reversed" means here. As described in appendix A, to convert the advection–diffusion equation to its adjoint, $\partial_t \to -\partial_t$ and $\mathbf{v} \cdot \boldsymbol{\nabla} \to -\mathbf{v} \cdot \boldsymbol{\nabla}$, while $\boldsymbol{\nabla} \cdot (\kappa\rho\boldsymbol{\nabla})$ remains unchanged. One might at first think that the physical effects of diffusion are, therefore, different. However, $G_0^\dagger(\mathbf{r}', t_0\,|\,\mathbf{r}, t)$ in (13) represents the mixing ratio resulting from a unit mass injected at $(\mathbf{r}, t)$ evolving under $(-\partial_{t_0} + \mathcal{T}^\dagger)G_0^\dagger(\mathbf{r}', t_0\,|\,\mathbf{r}, t) = \delta^3(\mathbf{r} - \mathbf{r}')\delta(t - t_0)/\rho$, with the causality condition that $t_0 \leq t$, so that the time parameter t_0 must actually run backward (continually decrease). Thus, the transport in the time-reversed flow represented by $G_0^\dagger(\mathbf{r}', t_0\,|\,\mathbf{r}, t)$ evolves under reversed velocities $(\mathbf{v} \to -\mathbf{v})$, but diffusion disperses tracer from a point source to a "cloud" just as it does in the time-forward flow.

We are now in a position to give $\mathcal{G}'$ a fresh interpretation. Since (12) defines $\mathcal{G}'$ as the Ω-integrated flux G', the transit-time pdf $\mathcal{G}'$ is the net flux of $G_0^\dagger(\mathbf{r}', t'\,|\,\mathbf{r}, t)$ out of the domain. From tracer-mass continuity it, therefore, also follows that

$$\mathcal{G}'(\mathbf{r}, t\,|\,\Omega, t') = \partial_{t'} M_0^\dagger(t'\,|\,\mathbf{r}, t), \quad (14)$$

where $M_0^\dagger(t'\,|\,\mathbf{r}, t) \equiv \int dm'\; G_0^\dagger(\mathbf{r}', t'\,|\,\mathbf{r}, t)$ is the probability that a tracer-marked particle released into the time-reversed flow at $(\mathbf{r}, t)$ will still be marked at time t', with $t > t'$. Since the flux of probability leaving through Ω at time t is the probability of arriving at Ω between time t and $t + dt$, $\mathcal{G}'$ has the natural interpretation of being the pdf of times for a tracer particle released at $(\mathbf{r}, t)$ into the time-reversed flow to "first" make contact with Ω. For the time-forward flow, $\mathcal{G}'$ is, therefore, the pdf of times since a particle arriving at $(\mathbf{r}, t)$ had *last* contact with Ω. We shall return to a more direct physical demonstration of the fact that fluxes of G_0 into Ω are

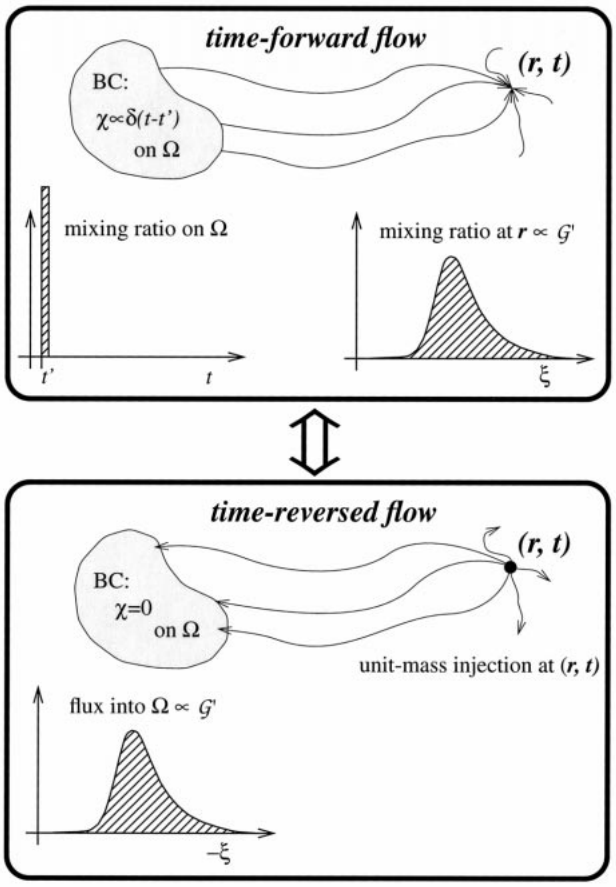

FIG. 6. Schematic illustration of two equivalent ways in which one can obtain the pdf, $\mathcal{G}'$, of times, ξ, since fluid at $(\mathbf{r}, t)$ was last in contact with some arbitrary fixed surface, Ω, indicated by the shaded region. (top) The time-forward flow. If a tracer mixing ratio on Ω is specified to be an impulse at t' proportional to $\delta(t - t')$, then the time evolution of the resulting mixing ratio at $\mathbf{r}$ as a function of elapsed time, $\xi = t - t'$, is proportional to $\mathcal{G}'(\mathbf{r}, t' + \xi | \Omega, t')$. (bottom) The equivalent situation in the time-reversed flow where zero-mixing-ratio BCs are imposed on Ω. A unit mass injected at $(\mathbf{r}, t)$ results in a net flux into Ω at a time $\xi = t - t'$ earlier (since time runs backward). This net flux is proportional to $\mathcal{G}'(\mathbf{r}, t | \Omega, t - \xi) = \mathcal{G}'(\mathbf{r}, t' + \xi | \Omega, t')$.

transit-time distributions when we consider tracer age below.

The relationships (13) and (14) represent one of the main results of this work, and their physical content is summarized schematically in Fig. 6. The pdf of times since fluid at $\mathbf{r}$ had *last* contact with Ω can be obtained either as the response at $\mathbf{r}$ to a δ-function BC over Ω in the time-forward flow, or in the time-reversed flow as the flux into Ω resulting from a unit mass injection at $\mathbf{r}$ when χ0BCs are imposed on Ω. As will be derived from a more fundamental point of view in section 4, the ''adjoint'' of this statement is similarly true. The pdf of transit times for fluid at $\mathbf{r}$ to make *first* contact with Ω can be obtained as either the flux into Ω resulting from a unit-mass injection at $\mathbf{r}$ under χ0BCs in the time-forward flow, or as the response at $\mathbf{r}$ to a δ-function BC over Ω in the time-reversed flow.

The relationship (13) between G' and G_0 can be expressed in another useful form when one writes the gradient as a limit and uses the reciprocity condition and the fact that when $\mathbf{r}_0$ is on Ω, $G_0(\mathbf{r}, t | \mathbf{r}_0, t') = 0$:

$$G'(\mathbf{r}, t | \mathbf{r}_0, t_0) = \rho(\mathbf{r}_0, t_0)\kappa(\mathbf{r}_0, t_0) \lim_{\epsilon \to 0} G_0(\mathbf{r}, t | \mathbf{r}_0 - \hat{\mathbf{n}}\epsilon, t_0)/\epsilon. \quad (15)$$

Thus, G_0 is essentially proportional to G' in the limit as the source point is close to Ω. The closer $\mathbf{r}_0$ gets, the more tracer of the initial unit injection of G_0 is lost, but this is compensated by scaling G_0 with $1/\epsilon$ so that G' remains normalized as in (11). For the simple 1D atmosphere of appendix B, (15) takes the form $G'(z, \xi) = \lim_{z' \to 0} G_0(z, z', \xi)/z'$ and a plot of G_0/z' with $z' = 0.001$ is indistinguishable from G' in Fig. 3.

A relationship between the probability M_0 and the pdf M' follows by integrating (13) with respect to dm, giving

$$M'(t | \mathbf{r}_0, t_0) = -\rho(\mathbf{r}_0, t_0)\kappa(\mathbf{r}_0, t_0)\hat{\mathbf{n}} \cdot \nabla_{\mathbf{r}'} M_0(t | \mathbf{r}', t_0)|_{\mathbf{r}' = \mathbf{r}_0}. \quad (16)$$

The spatial structure of M_0 with respect to the source location $\mathbf{r}'$ has consequences for M'. Note that as $\xi = t - t' \to 0$, the probability, M_0, of finding a marked particle in the atmosphere is unity (for short enough ξ there is no chance of having lost the tracer to the boundary; see also Fig. 4), except for the case where $\mathbf{r}'$ is right on Ω, that is, as $\xi \to 0$, the probability $M_0(t | \mathbf{r}', t - \xi)$ abruptly goes from unity to zero when $\mathbf{r}'$ reaches Ω. Thus, (16) implies that as $\xi \to 0$, $M'(t_0 + \xi | \mathbf{r}_0, t_0) \to \infty$ since the gradient of M_0 sees a sharp discontinuity at Ω. The boundary propagator G' has, therefore, an infinite initial pseudo mass, M', and the population particle-age pdf $P(t | t') = \int_\Omega d^2\,\mathbf{r}_0 M'/M_A$ is also singular at $t = t'$. This is an expression of the fact that a fluid particle ''released'' from Ω has overwhelming probability for immediately crashing into Ω again.

We were able to relate G_0 and G' through a simple differential operator because G_0 and G' have compatible BCs. However, G and G_0 (and hence G and G') obey different BCs and we know of no direct way of obtaining one from the other by applying a differential operator. Nevertheless, G and G' can be related by considering either that (a) the evolution of G over the control surface, Ω, can be propagated throughout the domain using G'; or that (b) G' can be regarded as a ''pseudo mixing ratio'' whose fluxes through Ω can be used to obtain G' everywhere using G. The integral equations connecting G and G' follow from the general solution (4) and may be used to derive approximate relationships, but this is not pursued further here.

3. Tracers as clocks and tracer-age distributions

We now develop the concept of a distribution of literal tracer age, which has concrete interpretation for arbitrary sources, and which forms the foundation for a direct physical construction of tracer-independent transit-time pdf's. Fluid marked by tracer naturally contains transit-time information. Consider a parcel at $(\mathbf{r}, t)$ with some tracer mixing ratio. If the source of that tracer was only ''on'' for a short burst at $(\mathbf{r}', t')$, we know that any tracer we find has age $t - t'$. This is the basic idea of ''tracer age.'' Note that this tracer age does not generally date the parcel under consideration as having been at $\mathbf{r}'$ at time t' because tracer-marked fluid will generally have been mixed via (turbulent) diffusion with unmarked (''clean'') fluid on the way from $\mathbf{r}'$ to $\mathbf{r}$. Tracer age is only the transit time of marked particles. Since our interest here lies in using tracers to extract flow characteristics, in section 4 we will explore under what circumstances tracer-age and transit-time distributions coincide.

Given a tracer source extending over space and time, and either zero-flux or χ0BCs, tracer age is naturally defined as follows. The tracer mixing ratio at the current time, t, is the mixture of tracer mass released at different times, t', in the past from various locations $\mathbf{r}'$. Imagine giving each fluid particle a clock that is started at the time it is marked with tracer at the source so that the particles marked between time t' and $t' + dt'$ will have ''clock time,'' or age, $t - t'$. (For example, one could imagine fluid elements labeled by a radioactive decaying isotope, which acts as a clock.) The mixing ratio of the collection of particles released between time t' and $t' + dt'$ is simply $dt' \int dm'\ G_x(\mathbf{r}, t\,|\,\mathbf{r}', t')S(\mathbf{r}', t')$, where G_x is either G (zero-flux BC) or G_0 (χ0BC). Therefore, the fraction of tracer mass residing in a volume V that has been in the flow for time $t - t'$ is given by $dt'\,Z(\mathbf{r}, t\,|\,S, t')$, where

$$Z(V, t\,|\,S, t') \equiv \frac{\displaystyle\int_V dm \int dm'\ G_x(\mathbf{r}, t\,|\,\mathbf{r}', t')S(\mathbf{r}', t')}{\displaystyle\int_V dm\ \chi(\mathbf{r}, t)}. \tag{17}$$

Hence, the average clock time (the mean tracer age) of the particles residing in V is given by

$$A(V, t, t_0) = \int_{t_0}^{t} dt'\ (t - t')Z(V, t\,|\,S, t'), \tag{18}$$

where we assumed that $S(\mathbf{r}', t') = 0$ for $t' < t_0$. Note that, by construction, the weighting function, Z, integrates to unity, $\int_{t_0}^{t} dt'\ Z(V, t\,|\,S, t') = 1$, so that we may think of Z as the distribution of clock times, $t - t'$, present in the volume V. We, therefore, refer to Z as a tracer-age distribution, which reduces to a transit-time pdf only under special conditions.

It is useful to have a completely local definition of the tracer-age distribution, which is obtained by taking the limit as the volume V shrinks to a point at $\mathbf{r}$, giving

$$Z(\mathbf{r}, t\,|\,S, t') \equiv \frac{1}{\chi(\mathbf{r}, t)} \int dm'\ G_x(\mathbf{r}, t\,|\,\mathbf{r}', t')S(\mathbf{r}', t'). \tag{19}$$

As defined by (19), $dt'Z$ is the mass fraction of tracer of age $t - t'$ that comprises the mixing ratio of the parcel at $\mathbf{r}$. Correspondingly,

$$A(\mathbf{r}, t, t_0) = \int_{t_0}^{t} dt'\ (t - t')Z(\mathbf{r}, t\,|\,S, t'), \tag{20}$$

defines the mean tracer age at $\mathbf{r}$.

The formulation of (17) and (19) relied on χ being determined through an interior source, S, and not through the imposition of any nonzero BCs on mixing ratio. This is not a loss of generality since we can always determine a source–sink field arbitrarily close to the surface that results in the desired surface mixing ratios. (For specified mixing ratios, this requires solving an inverse problem, but for complete surface information, the corresponding implied surface sources are in principle determined.)

As can be seen from (17) and (19), Z depends on the space and time dependence of the sources. The character of Z also depends strongly on whether zero-flux or zero-mixing-ratio BCs are imposed. Making an analogy with population dynamics, clocks are born at a certain rate at the sources and form a ''population'' showing various times/ages. Without a ''death'' process, the population just keeps on aging and mean tracer age increases without bound. This is the case when we impose zero-flux BC ($G_x = G$); once a clock is born it will tick forever. (As we shall see, the spatial structure of the ever increasing mean tracer age, A, carries useful transport information, but Z will not approach a stationary state as $t - t' \to \infty$.) If $G_x = G_0$, clocks making contact with the χ0BC control surface effectively die and the population of clocks reaches a statistically stationary age distribution as $t - t' \to \infty$.

4. Explicit construction of transit-time pdf's

To make the connection between the tracer-age distribution, and the pdf of transit times from a point $\mathbf{r}_A$ to some control surface, Ω (which could be shrunk to a point), we consider some idealized experiments. We can straightforwardly obtain the pdf of transit times if we release clocks at a steady rate at $\mathbf{r}_A$, measure their times as they reach Ω, and then, after measurement, remove the clocks from the system. A normalized histogram of the times recorded is then the pdf of $\mathbf{r}_A$-to-Ω transit times, denoted here by Z_T. Removal of clocks is important since otherwise one will eventually measure the time of clocks that had previously visited Ω.

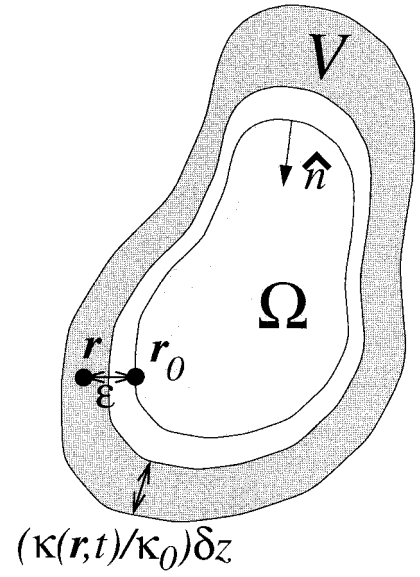

FIG. 7. Schematic of the construct to demonstrate the equivalence between the tracer-age distribution, Z, computed for the volume, V, and the flux into the control surface, Ω. As discussed in section 4, we take the limit as the thickness of V (chosen to be proportional to the diffusivity, κ) goes to zero, followed by a collapse of the resulting thin shell onto Ω as $\epsilon \to 0$.

Note that the transit times discussed here are not merely the Lagrangian transit times of the flow, but transit times determined by the subtle combination of advection and (turbulent) diffusion. Even without explicit advection, tracer-marked particles can still diffuse from $\mathbf{r}_A$ to any other point.

An idealized tracer experiment to accomplish the desired time keeping feat is constructed as follows: Place a constant source of tracer at $\mathbf{r}_A$ and impose χ0BC over Ω to remove clocks after measurement. We must now deal with the subtlety of the fact that right on the surface there is no tracer and hence no clocks. Fortunately, however, we can measure clock times at points $\mathbf{r}$ close to points $\mathbf{r}_0$ on Ω and take the limit as $\mathbf{r} \to \mathbf{r}_0$. It is useful to construct our histogram of clock times in terms of the mass fraction residing in a specified volume V as discussed in the previous section. We take V to be a shell surrounding Ω and then take the limit as the shell has zero thickness followed by the limit of moving this shell onto the surface Ω. The precise result we obtain depends on the details of how we take the limit of the shell collapsing to zero thickness. In order to connect with the results of section 2 relating boundary propagators to fluxes, it is useful to define the shell, V, such that its thickness is proportional to the local diffusivity κ. In the limit as V becomes a thin shell, the integral, $\int_V dm$, then becomes the surface integral, $(\delta z/\kappa_0)\int_{\partial V} d^2r\, \rho(\mathbf{r}, t)\kappa(\mathbf{r}, t)$, where z is the coordinate normal to the shell surface, κ_0 is an arbitrary constant, and ∂V can be taken as the inner surface of V. This setup is schematically illustrated in Fig. 7.

Thus, with $\rho(\mathbf{r}, t)S(\mathbf{r}, t) = \text{const.} \times \delta^3(\mathbf{r} - \mathbf{r}_A)\Theta(t - t_0)$ the distribution of clock times for the thin shell, V, is obtained from (17) as $Z_{\mathcal{T}}(\Omega, t \mid \mathbf{r}_A, t') \equiv \lim_{V\to\Omega} Z(V, t \mid S, t')$, that is,

$$Z_{\mathcal{T}}(\Omega, t|\mathbf{r}_A, t') = \lim_{V\to\Omega} \frac{\displaystyle\int_{\partial V} d^2r\, \rho(\mathbf{r}, t)\kappa(\mathbf{r}, t)G_0(\mathbf{r}, t|\mathbf{r}_A, t')}{\displaystyle\int_0^{t-t_0} d\xi \int_{\partial V} d^2r\, \rho(\mathbf{r}, t)\kappa(\mathbf{r}, t)G_0(\mathbf{r}, t|\mathbf{r}_A, t-\xi)}, \tag{21}$$

for $t \geq t' \geq t_0$. Equation (21) encapsulates a very direct and physical construct for the pdf of $\mathbf{r}_A$-to-Ω transit times. Clocks are born at $\mathbf{r}_A$, the flow takes them to their deaths at Ω, and we make a histogram of their ages just before death. We can now express $Z_{\mathcal{T}}$ in terms of tracer fluxes, because for $\mathbf{r}_0$ on Ω we have $G_0(\mathbf{r}_0, t|\mathbf{r}_A, t') = 0$, so that with $\mathbf{r} = \mathbf{r}_0 - \epsilon\hat{\mathbf{n}}$ we have $\lim_{\epsilon\to 0} G_0(\mathbf{r}_0 - \epsilon\hat{\mathbf{n}}, t|\mathbf{r}_A, t')/\epsilon = \hat{\mathbf{n}}\cdot\nabla_{\mathbf{r}} G_0(\mathbf{r}, t|\mathbf{r}_A, t')|_{\mathbf{r}=\mathbf{r}_0}$. Dividing both numerator and denominator of (21) by ϵ and taking the limit $\epsilon \to 0$, so that $\mathbf{r} \to \mathbf{r}_0$, and $V \to \Omega$, we obtain

$$Z_{\mathcal{T}}(\Omega, t|\mathbf{r}_A, t') = \frac{\mathcal{G}'^{\dagger}(\Omega, t|\mathbf{r}_A, t')}{\displaystyle\int_0^{t-t_0} d\xi\, \mathcal{G}'^{\dagger}(\Omega, t|\mathbf{r}_A, t-\xi)}; \qquad t \geq t' \geq t_0, \tag{22}$$

where we define $\mathcal{G}'^{\dagger}(\Omega, t|\mathbf{r}_A, t') \equiv \int_\Omega d^2r_0\, G'^{\dagger}(\mathbf{r}_0, t|\mathbf{r}_A, t')$, with

$$G'^{\dagger}(\mathbf{r}_0, t|\mathbf{r}_A, t') \equiv -\rho(\mathbf{r}_0, t)\kappa(\mathbf{r}_0, t)\hat{\mathbf{n}}\cdot\nabla_{\mathbf{r}} G_0(\mathbf{r}, t|\mathbf{r}_A, t')|_{\mathbf{r}=\mathbf{r}_0}, \tag{23}$$

which is the flux of G_0 into Ω at $\mathbf{r}_0$.

Through (22) our original explicit construct of $Z_{\mathcal{T}}$ as a histogram of clock times for tracer-marked particles from a constant source leads to a complementary interpretation. Expression (22) establishes the distribution, $Z_{\mathcal{T}}$, of times to *first contact* with Ω as the normalized net flux into Ω from a unit-mass injection at $\mathbf{r}_A$. Since this flux integrated over all time just gives unity, we can take the limit $t_0 \to -\infty$ in (22) to obtain the asymptotic $\mathbf{r}_A$-to-Ω transit-time pdf as

$$Z_{\mathcal{T}}(\Omega, t|\mathbf{r}_A, t') = \mathcal{G}'^{\dagger}(\Omega, t|\mathbf{r}_A, t'); \qquad t \geq t' > -\infty. \tag{24}$$

From conservation of mass it follows that

$$\mathcal{G}'^{\dagger}(\Omega, t|\mathbf{r}', t') = -\partial_t M_0(t|\mathbf{r}', t'). \tag{25}$$

Note that here χ0BC's are imposed on the destination surface, Ω, and the limit is taken as the *field* point, $\mathbf{r}$, approaches Ω. This contrasts to what is involved in the limit (15) relating G_0 to G' (and hence to $\mathcal{G}'$), where the *source* point approaches Ω. Also, the interpretation

of $\mathcal{G}'$ given in section 2c, was the distribution of transit times since *last* contact with Ω.

To establish the relation between $\mathcal{G}'$ and an explicit construct of the pdf of transit times we proceed as follows. Instead of using tracers to probe the flow, which is evolving forward in time, we can equally well imagine using tracers to probe the time-reversed flow (represented by the adjoint operator $\mathcal{T}^\dagger$). We can keep track of transit times in the time-reversed flow through the same construct as in the forward flow. Release clocks with a constant source $\rho(\mathbf{r}, t)S(\mathbf{r}, t) = \text{constant} \times \delta^3(\mathbf{r} - \mathbf{r}_A)$ into the time-reversed flow at $\mathbf{r}_A$, and impose χ0BC over Ω. We construct the distribution of (negative) clock times, $Z_{\mathcal{T}^\dagger}(\mathbf{r}_A, t\,|\,\Omega, t')$, in exactly the same way as in the case of the forward flow except that we use $G_0^\dagger$ instead of G_0 and time runs backward. Paralleling the steps that led to (22) using (15) and the reciprocity relation for $G_0^\dagger$, we find that

$$Z_{\mathcal{T}^\dagger}(\mathbf{r}_A, t\,|\,\Omega, t') = \frac{\mathcal{G}'(\mathbf{r}_A, t\,|\,\Omega, t')}{\displaystyle\int_0^{t-t_0} d\xi\, \mathcal{G}'(\mathbf{r}_A, t\,|\,\Omega, t-\xi)}; \; t \geq t' \geq t_0, \quad (26)$$

where $\mathcal{G}'$ is the net flux in the time-reversed flow into Ω resulting from a unit-mass injection at $\mathbf{r}_A$. The time integral of this flux is again normalized [cf. (11) and (12)] so that in the limit $t_0 \to -\infty$, we have

$$Z_{\mathcal{T}^\dagger}(\mathbf{r}_A, t\,|\,\Omega, t') = \mathcal{G}'(\mathbf{r}_A, t\,|\,\Omega, t'); \qquad t \geq t' > -\infty. \quad (27)$$

Since $Z_{\mathcal{T}^\dagger}$ is the distribution of times to first contact with Ω in the time-reversed flow, in the forward-evolving flow, $Z_{\mathcal{T}^\dagger}$ is the distribution of times since *last* contact with Ω.

Generally the pdf's $\mathcal{G}'$ and $\mathcal{G}'^\dagger$ are *not* equivalent. A sufficient condition for their equivalence is that $G_0(\mathbf{r}, t\,|\,\mathbf{r}', t-\xi) = G_0^\dagger(\mathbf{r}, -t\,|\,\mathbf{r}', \xi - t)$, which is true only in special cases such as pure diffusion without advection (see, e.g., MF53). The general nonequivalence of $\mathcal{G}'$ and $\mathcal{G}'^\dagger$ can be seen from the following example. Take the case where Ω is a small bubble. Suppose this Ω is connected via a closed stream line to point $\mathbf{r}_A$, with flow from Ω to $\mathbf{r}_A$ via a short segment of stream line and from $\mathbf{r}_A$ back to Ω via a much longer circuitous segment, and with flow speed roughly constant along the stream line. In this case, the mean time since particles at $\mathbf{r}_A$ had last had contact with Ω is shorter than the mean time for particles leaving $\mathbf{r}_A$ to make first contact with Ω, so that $\mathcal{G}' \neq \mathcal{G}'^\dagger$.

Consider the limit as Ω is shrunk to a point, say $\mathbf{r}_B$. In this limit, $\mathcal{G}'$ and $\mathcal{G}'^\dagger$ are perfectly well defined as the pdf's of A-to-B transit times, but their first and higher moments turn out to be infinite. As we have shown, $\mathcal{G}'$ and $\mathcal{G}'^\dagger$ are the time-dependent fluxes into Ω resulting from a unit mass injected at $\mathbf{r}_A$ into the time-reversed and time-forward flows, respectively. As the surface area of Ω is decreased, it takes increasingly long for the unit mass to escape through Ω. Because the total mass exiting through Ω is equal to the unit mass initially injected, regardless of the size of Ω, $\mathcal{G}'$ and $\mathcal{G}'^\dagger$ remain normalized in the point limit. However, in appendix C section b we show that for 2D and 3D purely diffusive transport, the mass flux out of Ω decays so slowly in the point limit that the first and higher moments of the transit-time pdf's diverge as Ω vanishes, even for a finite domain. This result generalizes to any advective-diffusive transport because diffusion dominates at small enough spatial scales. Although in the literature one finds point-to-point mean transit times discussed as though they were finite (see, e.g., Plumb and McConalogue 1988; HP94), from the results of appendix C section b, as well as from arguments made in the following section, we conclude that point-to-point mean transit times are infinite.

It is important to note that the divergence of the point A-to-B mean transit time does *not* imply that it will take an infinite time for a unit-mass injection at $\mathbf{r}_A$ to produce a finite mixing ratio (i.e., any finite fraction of G_∞) at $\mathbf{r}_B$ or any other point, $\mathbf{r}$. The characteristic ''mixing time,'' τ, for $\chi(\mathbf{r}) \sim G_\infty$ is finite for a finite reservoir, and represents the time when the majority of marked fluid particles have had a chance to visit $\mathbf{r}$. This contrasts with the mean transit time, which is computed as the mean over all particles binned according to their transit time. Because the majority of particles arrive at $\mathbf{r}$ in a time on the order of τ, the transit-time pdf has its peak around τ and the divergent moments are, therefore, attributable to slowly decaying tails for large $\xi = t - t'$ representing ''stragglers'' taking arbitrarily long to find their point target of Ω (in either the forward or time-reversed flow).

5. Transit time information from geophysical tracers

We now discuss how, and under what conditions, tracer-independent transit-time information can be extracted from geophysical tracers. For any flow and any source of tracer, we can always define the tracer-age distribution, Z, and mean tracer age, A, for every point in the domain. Unless Z is computed at special locations under the particular conditions examined in the previous section, Z will not coincide with either $\mathcal{G}'^\dagger$ or $\mathcal{G}'$. However, Z can still contain information on the mean transit time $\Gamma(\mathbf{r}, t) \equiv \int_{-\infty}^{t} dt'\,(t - t')\mathcal{G}'(\mathbf{r}, t\,|\,\Omega,\ t')$ since last contact with the control surface, Ω. One way to see this, is to compare the equations of motion for $\mathcal{G}'$ and Γ with those for Z and A. The equation for $\mathcal{G}'$ has the same form as that for G'; that is,

$$(\partial_t + \mathcal{T})\mathcal{G}' = 0, \quad (28)$$

with the BC $\mathcal{G}'(\mathbf{r}, t\,|\,\Omega,\ t') = \delta(t - t')$ for $\mathbf{r}$ on Ω. The equation for Γ follows as

$$(\partial_t + \mathcal{T})\Gamma = 1, \quad (29)$$

with the BC $\Gamma(\mathbf{r}, t) = 0$ for $\mathbf{r}$ on Ω, as noted by Boering et al. (1996). Equation (29) has in fact been used to define age (e.g., England 1995).

The equation for the locally defined tracer-age distribution, Z, may be written from its definition (19) as

$$(\partial_t + \mathcal{T})Z = [\delta(t - t') - Z]\frac{S}{\chi} - \frac{\mathcal{D}(Z, \chi)}{\chi}, \quad (30)$$

where for any two scalar fields, X and Y, we defined $\mathcal{D}(X, Y) \equiv \mathcal{T}(XY) - X\mathcal{T}(Y) - Y\mathcal{T}(X)$. The BC for Z follows from the BC for the corresponding G_x. The operator $\mathcal{D}$ represents diffusive coupling, which vanishes when $\mathcal{T}$ is a pure advection operator. The first moment of (30) gives the equation of motion for A:

$$(\partial_t + \mathcal{T})A = 1 - \frac{A}{\chi}S - \frac{\mathcal{D}(A, \chi)}{\chi}. \quad (31)$$

Thus, A and Γ differ through their equations of motion and, generally, also through their BCs. For the case of surface sources, $S = 0$ in the interior of the domain and (29) and (31) differ through the extra diffusive coupling $\mathcal{D}/\chi$ and the BCs.

We now consider several concrete geophysical examples and illustrate some of the concepts developed using numerical atmospheric transport models. Two models are used: the second-generation GCM of the Canadian Climate Centre (CCC) (McFarlane et al. 1992) and an offline chemical transport model (CTM) developed at the Goddard Institute for Space Studies (GISS) (Prather 1986; Prather et al. 1987). The CCC GCM is a spectral model of the troposphere with T32 horizontal resolution and 10 vertical levels to 10 mb. The tracer transport properties of this model have recently been studied in some detail (Holzer 1999). (For the case of surface BCs with spatial discontinuities, spectral transport produces Gibbs oscillations. For plotting only, lowest-level mixing ratios are, therefore, slightly filtered spatially.) The GISS CTM has a grid resolution of 7.8° lat, 10° long, and 21 vertical layers to 0.002 mb (~90 km) and is driven by a repeated single year of wind and convection data from a version of the GISS GCM with a full stratosphere (Rind et al. 1988). The GISS CTM has been used extensively to study stratospheric tracers (e.g., Hall and Prather 1995). Our purpose here is not to compare results between the two models but rather to illustrate the concepts developed using the model most appropriate for each particular case: CCC GCM for the troposphere and GISS CTM for the stratosphere.

a. Inferring mean transit times from tracer distributions: Constant surface sources, zero-flux BC

Suppose a tracer with no sinks is injected into the atmosphere with a constant source, that is, with $\rho(\mathbf{r}, t)S(\mathbf{r}, t) = s(\mathbf{r})\Theta(t - t_0)$, where $s(\mathbf{r})$ is constant over a patch, Ω, close to the earth's surface. The relevant Green function for this problem is G (zero-flux BC). Using this source in (20) with $G_x = G$ and taking the long-time limit $G \sim G_\infty$, we obtain that the mean tracer age $A \sim t/2$. This is intuitive; clocks initialized to zero are injected at a constant rate so that after a long time, t, their average clock time reads $(1/t)\int_0^t t'\, dt' = t/2$. Since we are pumping tracer into the atmosphere without any losses, the mixing ratio, χ, increases continuously. However, after a long time, χ can be decomposed into a linearly growing uniform background, χ_0, onto which is superposed a statistically stationary, spatially varying, state, χ^+, that is, $\chi = \chi_0 + \chi^+$, where $\chi_0 \equiv s_0 G_\infty t$ with $s_0 \equiv \int s(\mathbf{r})\, d^3r$ being the total mass injected per unit time.

The deviation $A^+(\mathbf{r}, t) \equiv A(\mathbf{r}, t) - t/2$ contains nontrivial transit-time information. In the limit of large t, A^+ obeys from (31)

$$(\partial_t + \mathcal{T})2A^+ = 1 - \frac{S}{s_0 G_\infty} - 2\frac{A^+ S}{\chi} - 2\frac{\mathcal{D}(A^+, \chi^+)}{\chi}, \quad (32)$$

where A^+ has zero-flux BCs. The coupling $\mathcal{D}(A^+, \chi^+)$ and A^+S are bounded, while χ grows like t, so that $\mathcal{D}/\chi$ and A^+S/χ vanish like $1/t$. Note that in the interior of the atmosphere, where $S = 0$, $2A^+$ and Γ obey the same equation once A^+S/χ and $\mathcal{D}/\chi$ are negligible. Recall that for Γ zero-mixing-ratio BCs are applied over Ω, with zero-flux BCs elsewhere. Thus, to the extent that $A^+(\mathbf{r}, t) \sim 0$ for $\mathbf{r}$ on Ω, we can consider $2A^+$ to obey the same BCs as Γ. It follows that

$$2\Delta A(\mathbf{r}, t) \cong 2A^+(\mathbf{r}, t) \cong \Gamma(\mathbf{r}, t), \quad (33)$$

with $\Delta A(\mathbf{r}, t) \equiv A(\mathbf{r}, t) - A(\Omega, t)$, where $A(\Omega, t)$ is the (area-weighted) average of A over Ω.

To calculate ΔA directly from the definition (20) of A, one needs to know G. Fortunately, however, it is straightforward to show that, in the limit $t - t_0 \to \infty$, the mixing ratio χ, resulting from the constant source, obeys the exact identity

$$2\Delta A = -\frac{\Delta\chi}{s_0 G_\infty}, \quad (34)$$

with $\Delta\chi(\mathbf{r}, t) \equiv \chi(\mathbf{r}, t) - \chi(\Omega, t)$, where $\chi(\Omega, t)$ is the average of χ over Ω. One can see this from (20) by taking $t - t_0$ large enough so that the integration range (t_0, t) can be split into two parts, (t_0, t_1) and (t_1, t), where the intermediate time, t_1, is chosen so that G is indistinguishable from G_∞ (to within some tolerance) over the interval (t_0, t_1). The spatial structure of χ thus comes from the interval (t_1, t), where G has temporal and spatial structure. Taking the limit of $A(\mathbf{r}) - A(\mathbf{r}_s)$ as $t_0 \to -\infty$ and averaging $\mathbf{r}_s$ over Ω gives (34). From (34) and (33) we have the useful relation

$$-\frac{\Delta\chi}{s_0 G_\infty} \simeq \Gamma, \quad (35)$$

which states that the mean transit time, Γ, is approxi-

mately equal to the time lag for $\chi(\mathbf{r}, t)$ to catch up to $\chi(\Omega, t)$.

How good is the approximation relating ΔA and $\Delta\chi$ to Γ as in (33) and (35)? We could also have arrived at (35) by using the general boundary propagator, G'. If we assume that χ over Ω is known, we can take it as a time-dependent BC on Ω (with zero flux elsewhere) and use (10)–(12) to obtain in the limit $t_0 \to -\infty$

$$\chi^+(\mathbf{r}, t) = -s_0 G_\infty \Gamma + \int_0^\infty d\xi \int_\Omega d^2 r_s \, G'(\mathbf{r}, t \,|\, \mathbf{r}_s, t - \xi) \times \chi^+(\mathbf{r}_s, t - \xi). \quad (36)$$

We recover (35) to the extent that $\int_0^\infty d\xi \int d^2\mathbf{r}_s \, G'\chi^+ \cong \chi^+(\Omega, t)$, which is exact only if χ^+ is uniform over Ω and time independent corresponding to a strictly uniform, linearly increasing BC over Ω, in which case (35) is obtained as an identity (HP94).

Equation (36) shows that the accuracy of approximation (35) hinges on how uniform χ^+ is over Ω, and how close χ^+ is to being time independent. For constant sources, near-surface mixing ratios can be expected to have a pronounced seasonal cycle, especially in the vicinity of the sources. Thus, it is only in a time average (e.g., over an annual cycle) that the mixing ratio's growth will be close to linear. However, for the time average (indicated by an overbar) of (36) to reduce to the time average of (35), we also need $\overline{G'\chi^+} \cong \overline{G'}\,\overline{\chi^+}$, or more precisely that $\overline{G'\,\chi^+} - \overline{G'}\,\overline{\chi^+}$ is small compared to $s_0 G_\infty \Gamma$, that is, that there is small covariance between the transport operator (represented in integral form by G') and the surface BC. Uniformity over Ω can be ensured by making Ω small enough, but in the limit as Ω is shrunk to a point, Γ and $2\Delta A$ will diverge as discussed in section 4.

The general case of a time-dependent, spatially distributed surface source is quite complicated and a full exploration of this case is beyond the scope of this paper. The difficulties associated with spatially distributed sources lie in the fact that there is no unique reference value to define easily interpreted lag times. We note that a spatially uniform source with time variation can be used to extract higher-order moments of the transit-time pdf.

We now illustrate the correspondence between Γ and $2\Delta A$ in the troposphere. The CCC GCM was used to simulate the mixing ratio resulting from (a) a constant source applied over a surface patch, Ω, and from (b) a BC on mixing ratio enforced over the same patch that increases linearly in time with rate γ (a ''ramp'' BC). To test our expectation of reasonable agreement between Γ and $2\Delta A$ for a small source patch and approximate agreement for extended sources, we performed simulations with two choices of patch size. For the small patch, we chose the 11 grid boxes of the model's 96×48 Gaussian grid within a radius of 790 km of the surface point (50.1°N, 11.3°W) in Europe. This patch has only 0.28% of the global surface area to demonstrate the divergence expected as sources become pointlike. The large patch is defined as the land surface of the Northern Hemisphere, excepting that of Africa and South America. In each case the model is run into quasi-stationary state, so that mixing ratio increases with the same average rate everywhere in the troposphere. For the constant sources this occurs after a time on the order of the tropospheric mixing time ($\sim$1 yr), but for the ramp-BC case one has to wait for several typical upper tropospheric Γ before the BC is propagated throughout the troposphere, which for the small patch necessitated runs of several decades. For the ramp-BC case, the mean transit time since last contact with the patch is given by $\Gamma = -\Delta\chi/\gamma$, and for the constant-source case $2\Delta A = -\Delta\chi/(s_0 G_\infty)$. The differential tracer age, $2\Delta A$, has a large seasonal amplitude (not shown) primarily due to the strong seasonality of A over the source region. We, therefore, present only annual averages here.

The results for the small patch are shown in Fig. 8. Note that $2\Delta A$ is on the order of 15 yr, much larger than the tropospheric mixing time. The shapes of the contours of $2\Delta A$ and Γ are virtually identical and their amplitudes agree to within 12%–15%. Given the small patch size, we attribute the differences between $2\Delta A$ and Γ to covariance between transport and surface mixing ratio [cf. (36)]. The fields on the lowest model level show the character of the divergence of Γ: steep gradients surround the source region, corresponding to high mixing ratios in that region. Away from the source region, the pattern of Γ is that of the characteristic stationary-state distribution of mixing ratio. We expect that in the limit of vanishing patch size, the ''hole,'' where Γ drops to zero at the source (corresponding to the peak in mixing ratio), becomes more sharply peaked, driving the characteristic values of Γ to ever higher values, but that the basic pattern of Γ away from the source region remains the same. Because the divergence is localized, it affects the zonal means to a lesser degree and the differences between the Southern Hemisphere values of Γ and those in the vicinity of the source latitude, represent characteristic tropospheric mixing times (Holzer 1999).

In the limit as Ω is shrunk to a point, the correspondence (35) between Γ and $2\Delta A$ affords new insight into the nature of the divergence (see appendix Cb). Physically, the cause of the divergence is clear in the point limit: a constant source continually deposits mass into an infinitesimal volume, resulting in infinite mixing ratio at the source, and hence infinite $\Delta\chi$ and ΔA.

The relatively good agreement between $2\Delta A$ and Γ for the small patch is to be contrasted with the results for the large patch shown in Fig. 9. In the constant source case the flow redistributes near-surface mixing ratio over Ω, so that there are regions where $\Delta A \equiv A - A(\Omega) < 0$. The variations of $2\Delta A$ over Ω are on the same order as the characteristic tropospheric values of $2\Delta A$. Consequently, $2\Delta A$ and Γ have large differences close to Ω and, even in the remote Southern Hemisphere

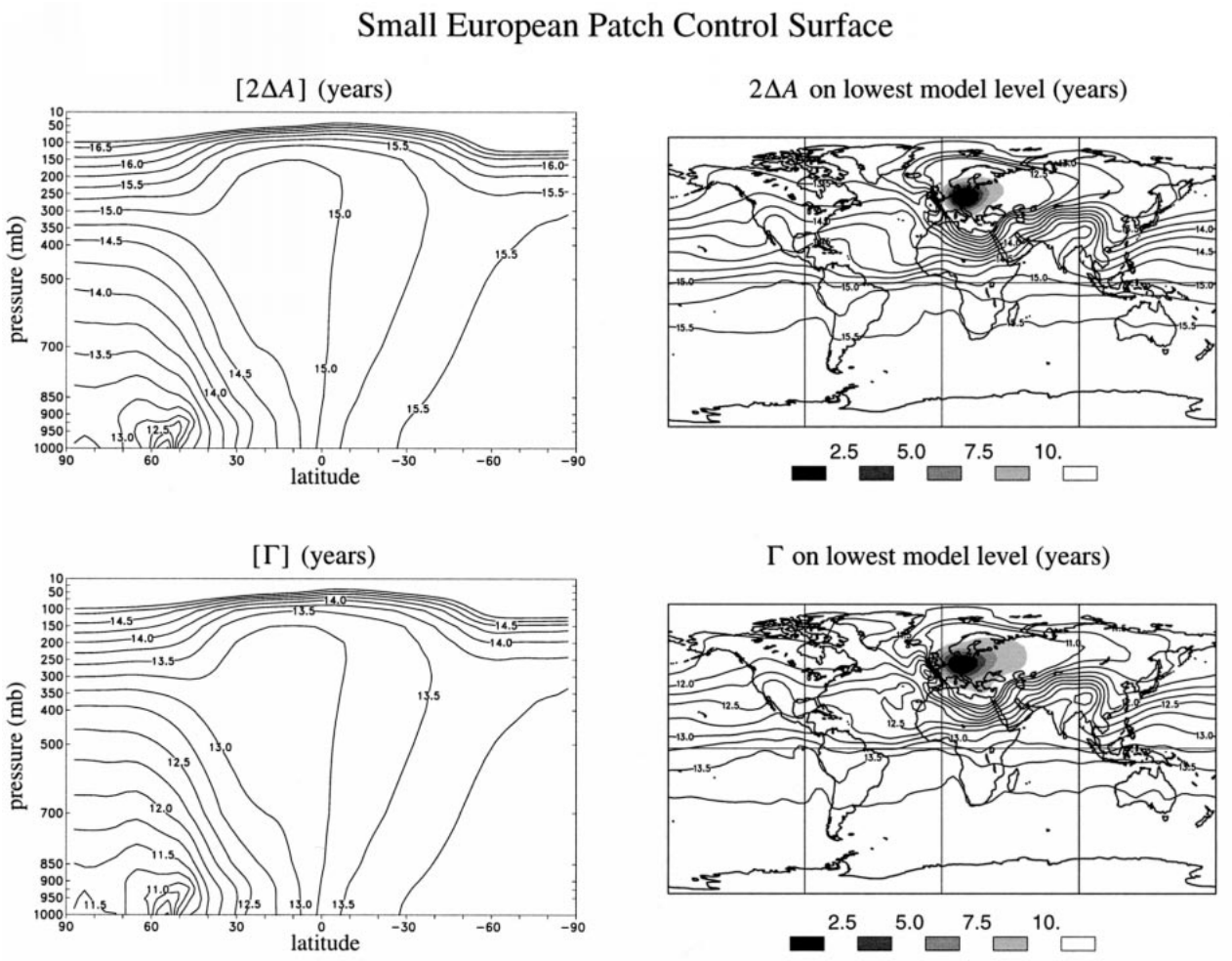

FIG. 8. Annual averages of the differential tracer age, $2\Delta A$, and the mean transit time, Γ, as simulated by the CCC GCM for the case of the control surface, Ω, being a small patch in Europe centered on (50.1°N, 11.3°W) with 0.28% of the global surface area. The tracer age was computed as $2\Delta A(\mathbf{r}, t) = [\chi(\Omega, t) - \chi(\mathbf{r}, t)]/(s_0 G_\infty)$ from the stationary-state mixing ratio, χ, resulting from a constant source over Ω. [The reference value, $\chi(\Omega, t)$, is the average of χ over Ω.] The transit time, Γ, was computed as $[\chi(\Omega, t) - \chi(\mathbf{r}, t)]/\gamma$ from the stationary-state mixing ratio resulting from the ramp BC, $\chi(\mathbf{r}_s, t) = \gamma t$ for $\mathbf{r}_s$ on Ω. The contour interval is 0.25 yr.

troposphere, the magnitudes of $2\Delta A$ and Γ differ by a factor of $\sim$1.5, although the contour shapes are similar. For this choice of Ω, both $2\Delta A$ and Γ are on the order of the tropospheric mixing time as expected, since this time should be on the same order as the time since last contact with the Northern Hemisphere surface.

b. Transit-time pdf's to first and since last surface contact: Interior source, zero-mixing ratio BC

Given a constant source in the interior of the geophysical reservoir, with χ0BC over some control surface, Ω, tracer age can be defined at any point $\mathbf{r}$, but does not everywhere reduce to a source-to-$\mathbf{r}$ transit time. Fluid particles are labeled with clocks at the source and these clocks are removed at Ω. A fluid particle is not assigned a new clock until it recirculates to the source. Thus, unlabeled fluid always mixes with labeled fluid and χ does not continually grow in time, so that $\mathcal{D}/\chi$ in Eq. (31) for A never vanishes. In terms of the flux picture of transit-time distributions, the flux from an interior pulse is only a transit-time pdf (the pdf to first contact) when it is the total flux into Ω. With this configuration it is, therefore, only possible to deduce the source-to-surface transit-time pdf.

Geophysical realizations of interior sources with approximate zero-mixing ratio BCs are provided by stratospheric emissions that rapidly rain out of the atmosphere upon reaching the lower troposphere. For example, the flux of radiocarbon out of the atmosphere in response to the stratospheric nuclear bomb tests of the 1950s contains information on the source-to-surface transit-time pdf. Aerosols from volcanic eruptions and long-lived emissions from high-flying aircraft may also provide such information, if their signals can be sufficiently separated from the background. For the oceans, one

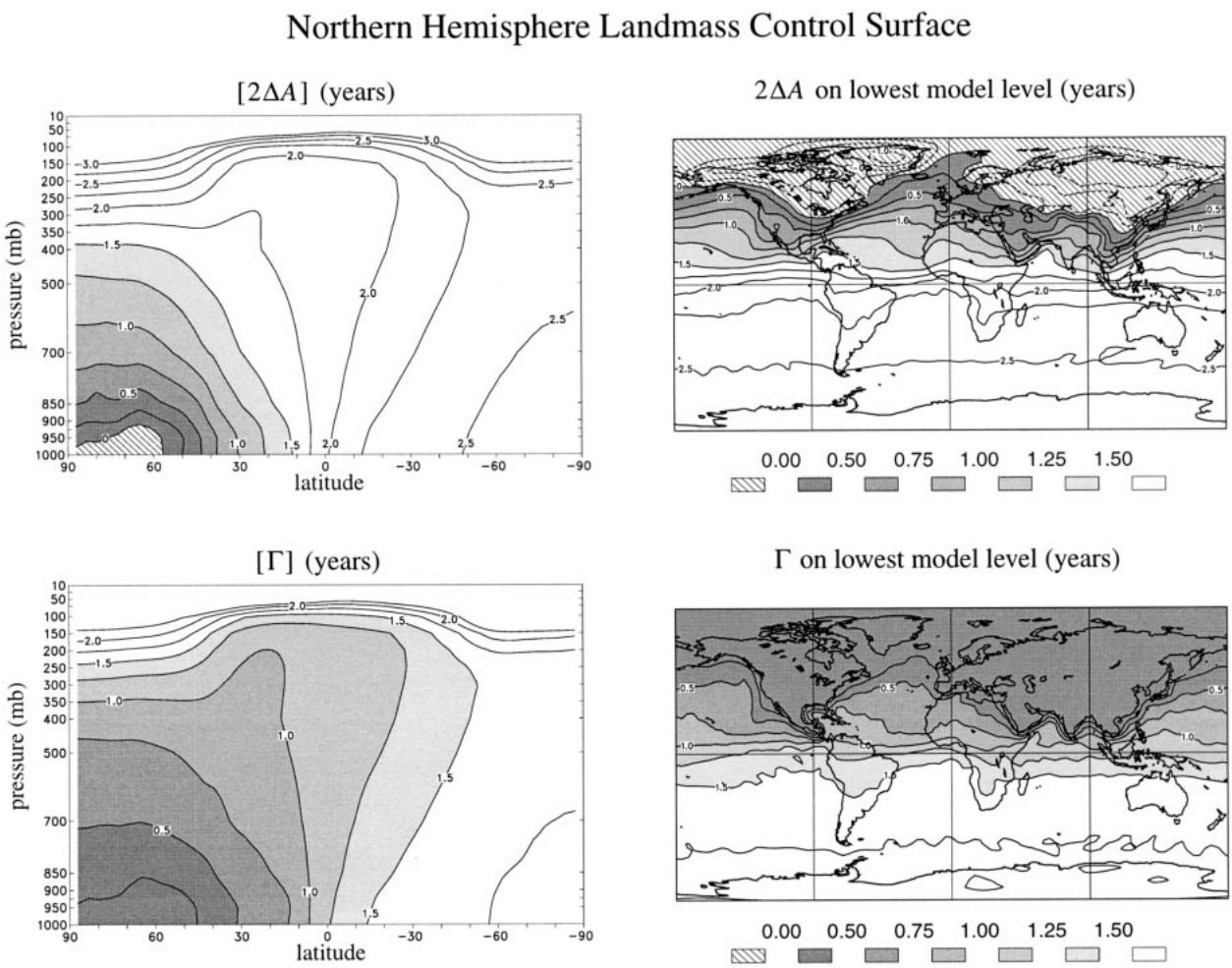

FIG. 9. As for Fig. 8 with Ω consisting of the Northern Hemisphere landmass except that of Africa and South America. (Note that the grayscale is different from that of Fig. 8.)

could imagine a man-made artificial release of some suitable tracer, with the atmosphere providing a uniform BC on the oceanic mixed layer concentration. The normalized net flux into the atmosphere as a function of time would be equivalent to the release-point-to-ocean-surface transit-time pdf.

Interior sources can easily be incorporated into numerical models of geophysical flows to extract transit times of interest. We demonstrate this by using the GISS CTM to explicitly generate G_0 for the source point $\mathbf{r} =$ (3.9°N, 175°W, 34 mb) in the lower tropical stratosphere with a χ0BC over the earth's surface (lowest model level). Spatially the source occupies a single CTM grid box (in the vertical from 46 to 22 mb), and in time the source is ''on'' for an entire month. Thus, the response to this source is a smoothed G_0 resulting from a convolution with a 1-month square pulse in time. We generate 12 such smoothed G_0, one for the source being on for each month of the year. The net flux into the earth's surface was computed from the tracer mass loss rate as $-\partial_t M_0(t|\mathbf{r}', t')$ [cf. (25)], which gives us the pdf, $\mathcal{G}'^{\dagger}$ of transit times to *first* contact with the surface. To contrast this against the pdf of transit times since *last* contact with the surface, we computed a smoothed $\mathcal{G}'$ by holding the mixing ratio in the lowest model level at unity for a 1-month period and thereafter enforcing χ0BC over the lowest model level. This was again done for 12 such month-long pulses in the surface BC, one for each month of the year. Monthly means of the resulting pdf's, $\mathcal{G}'(\mathbf{r}_A, t|\Omega, t')$ and $\mathcal{G}'^{\dagger}(\Omega, t|\mathbf{r}_A, t')$, are shown in Fig. 10 as a function of elapsed time $\xi = t - t'$, averaged over the 12 source times.

The pdf's $\mathcal{G}'$ and $\mathcal{G}'^{\dagger}$ are quite different, as may be expected. Air travels from the surface to the lower tropical stratosphere via efficient convective mixing in the tropical troposphere and vertical advection through the tropical lower stratosphere. The dominant paths from the surface to $\mathbf{r}$ through the tropical tropopause are, therefore, expected to have relatively short transit times compared to the paths leading from $\mathbf{r}$ to the surface,

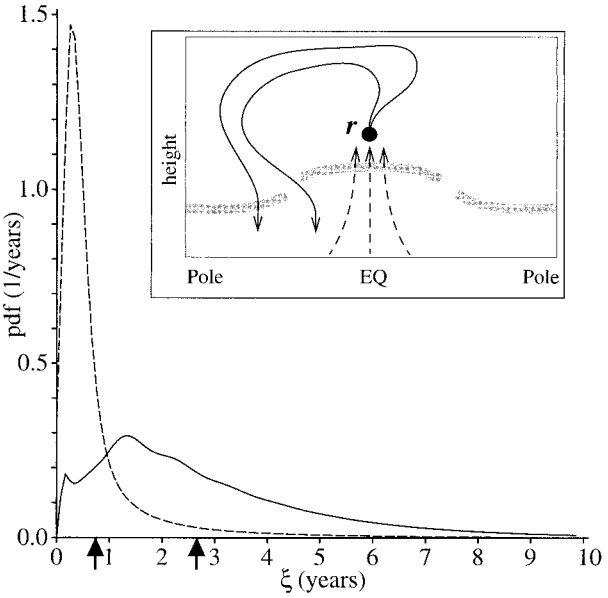

FIG. 10. The pdf of transit times, $\mathcal{G}'^{\dagger}$ (solid line), to first contact with the earth's surface from the point $\mathbf{r}$ = (3.9°N, 175°W, 34 mb) in the tropical lower stratosphere, and the pdf of transit times, $\mathcal{G}'$ (dashed line), at $\mathbf{r}$ since last contact with the earth surface, as simulated by the GISS CTM. The pdf $\mathcal{G}'$ was computed as the response to a 1-month, full-surface pulse BC. Twelve $\mathcal{G}'$ and $\mathcal{G}'^{\dagger}$ pdf's were computed with source and BC pulses for each month of the year. Shown is the dependence on elapsed time $\xi = t - t'$ averaged over the 12 source times. Arrows indicate a mean transit time of 0.74 yr for $\mathcal{G}'$, and of 2.66 yr for $\mathcal{G}'^{\dagger}$. The inset shows a schematic of zonally averaged atmospheric transport. The gray shading indicates the tropopause. The dashed arrows represent paths that contribute to $\mathcal{G}'$ and involve rapid tropical convection. The solid lines represent return paths from $\mathbf{r}$ back to the surface via the stratospheric circulation and stratosphere–troposphere exchange. The return paths contribute to $\mathcal{G}'^{\dagger}$.

which involve slow stratospheric circulation to the midlatitude tropopause where tracer then mixes with the troposphere again. Correspondingly, the pdf, $\mathcal{G}'$, of times since last surface contact has a relatively narrow peak at about 0.25 yr and a mean-transit time of 0.74 yr, while the pdf, $\mathcal{G}'^{\dagger}$, of times to first surface contact is much broader (indicating a greater multiplicity of pathways) with a peak at 1.3 yr and a mean-transit time of 2.7 yr.

c. *Nonstationary tracer age: An oceanic example*

In many geophysical examples mean transit times cannot be readily inferred from tracers because the tracer distribution is in a transient state. In such cases, not all fluid particles carry a tracer clock, so that observations in general represent averages over labeled and unlabeled fluid. Consider anthropogenic tracers, such as the CFCs, in the ocean. The atmospheric evolution of CFCs acts as a time-dependent BC at the ocean surface, which then propagates into the deep ocean. Most ocean water, however, has not made contact with the surface during the time CFCs have been present in the atmosphere, approximately the past 40 yr. Thus, there is ''clean'' ocean water available to mix with CFC-labeled water, preventing the interpretation of a CFC lag time as a mean transit time since last surface contact.

A technique to counter the dilution of tracer-labeled fluid makes use of the ratio of tracers, such as CFC-11/CFC-12, both of which have been present in the atmosphere for similar times (e.g., Haine and Richards 1995). The idea is to exploit the fact that the ratio of tracer concentrations in a water parcel is not affected by the presence of unlabeled water, which dilutes each tracer by an equal fraction. If the ratio of the effective sources of the two tracers at the ocean surface increases linearly in time, a simple interpretation of the tracer ratio follows. Taking $S_2(\mathbf{r}, t) = \gamma t S_1(\mathbf{r}, t)$, where γ is a constant rate, and using the definition (20) of mean tracer age, it is straightforward to derive that the tracer ratio, $R \equiv \chi_2/\chi_1$, is related to the tracer age, A_1, of χ_1 through

$$R = \gamma(t - A_1), \tag{37}$$

assuming no internal tracer sources and that both surface sources ''switched on'' at $t = 0$. Thus, R contains information on the mean transit time of χ_1-labeled fluid elements, but R will *not* be related to the flow's mean transit time since last surface contact until a statistical stationary response to the sources is achieved and the diffusive coupling term, $\mathcal{D}$, vanishes in Eq. (31) for A_1. This may take millennia in the deep ocean. How the stationary-sate mean tracer age, A_1, is related to the moments of the transit-time pdf depends on the structure of S_1. (The case of constant S_1 is discussed in section 5a.)

6. Summary and conclusions

To make the best use of the transport information provided by geophysical tracer observations and to interpret transport properties of numerical models, one needs a conceptual and analytical framework allowing clear physical interpretation. In this paper we have presented such a framework by defining the tracer-age distribution and exploring its relationship with transit-time pdf's using the passive-tracer Green function. The pdf of transit times $\mathcal{G}'$, since the fluid elements comprising a fluid parcel had last contact with a specified surface Ω (the age spectrum of HP94) was shown to be the Ω-integrated propagator, G', of arbitrary mixing-ratio BCs on Ω. By expressing G' in terms of the appropriate Green function, we found that $\mathcal{G}'(\mathbf{r}, t\,|\,\Omega,\ t')$ is the time series of flux into Ω resulting from a unit-mass injection at $(\mathbf{r}, t)$ into the time-reversed flow.

The Green function of the tracer transport equation allows one to decompose tracer mixing ratio into contributions injected into the flow at each time interval in the past. Tracer particles can thus be thought of as clocks that are started when they are injected into the flow. This simple idea led us to a natural and literal definition

of a tracer-age distribution, Z, and its mean, the mean tracer age, A, which are generally distinct from a transit-time pdf and a mean transit time for the flow. The tracer-age distribution, Z, bins the mass of clocks according to the time they read. We used Z to explicitly construct a pdf of transit times from some point $\mathbf{r}$ to a surface, Ω. With a constant source at $\mathbf{r}$ and a carefully chosen volume (surrounding Ω), for which mass fractions of a given clock time interval are computed, Z can be reduced to $\mathcal{G}'$. This construction gives a precise physical interpretation of $\mathcal{G}'(\mathbf{r}, t \,|\, \Omega,\ t')$ as the pdf of times since fluid at $\mathbf{r}$ had *last contact* with Ω and also establishes its adjoint, $\mathcal{G}'^{\dagger}(\Omega, t' \,|\, \mathbf{r}, t)$, as the pdf of times for fluid at $\mathbf{r}$ to have *first contact* with Ω. Except for purely diffusive flow, $\mathcal{G}'$ and $\mathcal{G}'^{\dagger}$ are generally not equivalent.

Using a the GISS CTM, we gave explicit examples of the pdf $\mathcal{G}'$ of transit times since air at a point $\mathbf{r}$ in the lower tropical stratosphere had last surface contact and the pdf $\mathcal{G}'^{\dagger}$ for air at $\mathbf{r}$ to have first surface contact. The two pdf's are markedly different. Transport to $\mathbf{r}$ from the surface is dominated by rapid tropical convection to the tropopause, followed by direct upward advection in the lower tropical stratosphere, while subsequent transport back to the troposphere involves the slower stratospheric circulation to reach the midlatitude tropopause. In this example $\mathcal{G}'^{\dagger}$ was obtained as the flux of tracer into the earth's surface resulting from a unit-mass injection at $(\mathbf{r}, t')$ with zero-mixing-ratio BCs over the earth's surface. If $\mathcal{G}'^{\dagger}$ were of interest for all $\mathbf{r}$ in the stratosphere (e.g., to obtain stratospheric residence times for tracer emitted at different locations), it would be impractical to simulate unit-mass injections from every point. However, because of the equivalence of $\mathcal{G}'^{\dagger}$ and a boundary propagator in the time-reversed flow, $\mathcal{G}'^{\dagger}$ could be computed at every point as a response to a pulse BC for the adjoint numerical model.

It is natural to consider point-to-point transit times. However, while the point-to-point transit-time pdf is well defined, its moments, including the mean transit time, are infinite in two and three dimensions. For a finite-sized reservoir such as the atmosphere, this infinite mean transit time does not imply that a unit mass released at $\mathbf{r}'$ will produce a finite mixing ratio at $\mathbf{r}$ only after an infinite time. The majority of tracer particles arrive at $\mathbf{r}$ after a finite time, but there are a sufficient number of particles taking arbitrarily long to find their point target of Ω to make the mean time for particles to have visited $\mathbf{r}$ via all possible paths infinite. This highlights the fact that any transit-time pdf not only depends on the flow but also on the geometry of the control surface, Ω, and the dimensionality of the problem. We note, however, that when Ω is a large, extended region, the transit times since last, and to first, Ω contact are not very sensitive to the geometry of Ω. For example, whether Ω is the entire earth's surface or just the Northern Hemisphere has only a minor impact on the mean transit time since last contact for stratospheric air parcels. Even though the magnitude of mean transit times sharply increases when Ω is shrunk to a small surface patch, we find that the *gradients* of the mean transit time are only affected in the vicinity of Ω. For example, stratospheric transit-time differences with respect to the tropical tropopause are insensitive to the size of a surface Ω.

To illustrate how transit-time information can be extracted from geophysical tracers, we compared the equations of motion for mean tracer age and mean transit time. In source-free regions, the equation for mean tracer age has an extra diffusive coupling, $\mathcal{D}$, between mixing ratio and mean tracer age. This coupling vanishes only when tracer is sampling all possible paths from the source to the point of interest. For a steady source and zero-flux BCs, the stationary-state mixing ratio referenced to the source region is directly proportional to mean tracer age similarly referenced to the source region. However, this differential mean tracer age is only approximately equal to the mean time since last contact with the source region. The approximation holds only for time averages long enough so that tracer from the constant source is increasing at an approximately steady rate at the source, to the degree that tracer is uniform over the source region, and to the degree that seasonal covariances between transport and mixing ratio at the source can be neglected. Using the CCC GCM, we demonstrated that this approximation holds to within $\sim 10\%$ when Ω is a small surface patch, but when Ω consists of the Northern Hemisphere landmass, the two measures of mean transit time differ by a factor of ~ 2 in the troposphere. The large discrepancy for extended source regions highlights the basic difficulty with extended sources that there is no unique reference value for defining easily interpretable lag times.

The distribution of anthropogenic tracers in the ocean is in a transient state, which prevents ''snapshots'' of tracer lag times from being interpreted as mean transit times. Consequently, ratios of tracers, such as CFC-11/CFC-12, are often resorted to for the extraction of transport timescales. Using the framework developed here, we have shown that for the special case, where the ratio of the sources increases linearly in time, the ratio of mixing ratios at a point $\mathbf{r}$ in the ocean has a concrete interpretation in terms of the mean tracer age since last surface contact. This tracer age has no simple relation to the moments of the transit-time pdf, because not all paths available to water from the surface to $\mathbf{r}$ have been sampled by tracer. Nonetheless, mean tracer age may be useful to help interpret constraints on ocean models.

We have given precise definitions and interpretations of transit-time and tracer-age distributions, and hope that the framework developed will be helpful in future investigations of geophysical transport. We have presented a few examples, but many issues remain to be explored. These include how best to deal with spatially extended sources, the detailed dependence of mean transit times on the size of the source region, the physics that sets the length scale over which a point source

sustains high gradients in the presence of turbulent flow, and generally an investigation of how different paths corresponding to different dynamical mechanisms contribute to the transit-time pdf. In addition to being useful in the context of the atmosphere, the framework of this paper may also help to interpret oceanic transport timescales inferred from tracers and tracer ratios having sources with various time variations. For example, natural radiocarbon, which has known atmospheric abundance due to cosmogenic generation and decays in the ocean with its isotopic half-life of 5568 yr, has been used to establish oceanic timescales (e.g., Broeker et al. 1988) that likely approximate mean transit times closely.

Acknowledgments. We thank Greg Flato and Ron Miller for enjoyable discussions on subtle aspects of diffusive transport. Tim Hall acknowledges support from the NASA Atmospheric Effects of Aviation Program.

APPENDIX A

General Solution and Advective-Diffusive Case

To derive the general solution of (1) in terms of G, we also need the equation of motion for the adjoint Green function, $G^\dagger(\mathbf{r}, t\,|\,\mathbf{r}_0, t_0)$, which takes tracer from $(\mathbf{r}_0, t_0)$ to $(\mathbf{r}, t)$ in the time-reversed flow. The equation for $G^\dagger$ is obtained by replacing $\mathcal{T}$ with its adjoint $\mathcal{T}^\dagger$ and reversing time, $t \to -t$ [see, e.g., Morse and Feshbach (1953), hereafter MF53)], which gives

$$(-\partial_t + \mathcal{T}^\dagger)G^\dagger(\mathbf{r}, t\,|\,\mathbf{r}_0, t_0) = \frac{1}{\rho(\mathbf{r}, t)}\delta^3(\mathbf{r} - \mathbf{r}_0)\delta(t - t_0). \tag{A1}$$

Following MF53, the general solution of (1) is now derived as follows. Multiply (1) with $\rho(\mathbf{r}, t)$ $G^\dagger(\mathbf{r}, t\,|\,\mathbf{r}', t')$ and (A1) by $\rho(\mathbf{r}, t)\chi(\mathbf{r}, t)$ and subtract the two resulting equations to obtain

$$\begin{aligned}\partial_t[\rho(\mathbf{r}, t)\chi(\mathbf{r}, t)G^\dagger(\mathbf{r}, t\,|\,\mathbf{r}_0, t_0)] &- \boldsymbol{\nabla}\cdot\mathbf{C}[G^\dagger(\mathbf{r}, t\,|\,\mathbf{r}_0, t), \chi(\mathbf{r}, t)] \\ &= \rho(\mathbf{r}, t)G^\dagger(\mathbf{r}, t\,|\,\mathbf{r}_0, t_0)S(\mathbf{r}, t) \\ &\quad - \chi(\mathbf{r}, t)\delta^3(\mathbf{r} - \mathbf{r}_0)\delta(t - t_0),\end{aligned} \tag{A2}$$

where we have defined

$$\begin{aligned}\boldsymbol{\nabla}\cdot\mathbf{C} = \rho(\mathbf{r}, t)[&\chi(\mathbf{r}, t)\mathcal{T}^\dagger G^\dagger(\mathbf{r}, t\,|\,\mathbf{r}_0, t_0) \\ &- G^\dagger(\mathbf{r}, t\,|\,\mathbf{r}_0, t_0)\mathcal{T}\chi(\mathbf{r}, t)] \\ &+ \chi(\mathbf{r}, t)G^\dagger(\mathbf{r}, t\,|\,\mathbf{r}_0, t_0)\partial_t\rho(\mathbf{r}, t),\end{aligned} \tag{A3}$$

and $\boldsymbol{\nabla}$, $\mathcal{T}$, and $\mathcal{T}^\dagger$ all act on $\mathbf{r}$. Equation (A3) may be considered a generalization of Green's theorem. Now integrate (A2) with respect to $\mathbf{r}$ over the entire domain and with respect to t from $t = 0$ to $t = t_0^+$, where t_0^+ is just slightly larger than t_0. Under this $dt\,d^3r$ integral, the last term of (A2) becomes $\chi(\mathbf{r}_0, t_0)$, which is then equal to

$$\begin{aligned}\chi(\mathbf{r}_0, t_0) = &\int d^3r\,\rho(\mathbf{r}, 0)\chi(\mathbf{r}, 0)G^\dagger(\mathbf{r}, 0\,|\,\mathbf{r}_0, t_0) \\ &+ \int_0^{t_0^+} dt\,\rho(\mathbf{r}, t)G^\dagger(\mathbf{r}, t\,|\,\mathbf{r}_0, t_0)S(\mathbf{r}, t) \\ &+ \int_0^{t_0^+} dt \int_\partial d^2r\,\hat{\mathbf{n}}\cdot\mathbf{C}[G^\dagger(\mathbf{r}, t\,|\,\mathbf{r}_0, t_0), \chi(\mathbf{r}, t)],\end{aligned} \tag{A4}$$

where we used the (adjoint) causality relation that $G^\dagger(\mathbf{r}, t_0^+\,|\,\mathbf{r}_0, t_0) = 0$, and replaced the volume integral of $\boldsymbol{\nabla}\cdot\mathbf{C}$ with the surface integral of $\hat{\mathbf{n}}\cdot\mathbf{C}$ over the boundary of the tracer domain (denoted by ∂). Now relabel variables $(\mathbf{r}_0, t_0) \to (\mathbf{r}, t)$ and $(\mathbf{r}, t) \to (\mathbf{r}', t')$ and express $G^\dagger$ in terms of G by using the reciprocity relation $G^\dagger(\mathbf{r}_1, t_1\,|\,\mathbf{r}_2, t_2) = G(\mathbf{r}_2, t_2\,|\,\mathbf{r}_1, t_1)$ to obtain (4) with $\mathbf{C}$ defined through (A3). (A reciprocity relation of this form generally holds for Green functions—for a derivation see, e.g., MF53.)

For the advective-diffusive transport operator (3) the adjoint is obtained by replacing $\mathbf{v}$ with $-\mathbf{v}$, while the diffusive operator remains unchanged. Substituting (3) and its adjoint into (A3), we obtain

$$\boldsymbol{\nabla}\cdot\mathbf{C}(\psi, \phi) = \boldsymbol{\nabla}\cdot[\kappa\rho(\psi\boldsymbol{\nabla}\phi - \phi\boldsymbol{\nabla}\psi) - \rho\mathbf{v}\psi\phi], \tag{A5}$$

where we made use of the fluid-mass continuity equation, $\partial_t\rho + \boldsymbol{\nabla}(\mathbf{v}\rho) = 0$. Using the form (A5) for $\boldsymbol{\nabla}\cdot\mathbf{C}$ in (A3) gives the general advection-diffusion boundary term (5).

APPENDIX B

Analytical Solutions for a Simple 1D Model

It is useful to demonstrate the relationships derived in section 2 in terms of explicit analytical solutions for a simple 1D diffusion model. Because of its simplicity, appropriateness to the atmosphere, and to make direct contact with the work of Hall and Plumb (1994, herafter HP94) we consider the model

$$\partial_t\chi - \rho^{-1}\kappa\partial_z\rho\partial_z\chi = S, \tag{B1}$$

where the height $z \geq 0$; the air density, ρ, has the form $\rho(z) = \rho_0\exp(-z/H)$; and the diffusivity κ, scale height H, and density scale ρ_0 are constants. We nondimensionalize (B1) via $z/H \to z$, $t(\kappa/H^2) \to t$, $\rho/\rho_0 \to \rho$. Since the transport operator here is constant in time, G, G_0, and G' are simple functions that can depend on time only through $\xi = t - t'$. The Green functions of (B1) are defined by replacing the source S with $\delta(\xi)\delta^3(\mathbf{r} - \mathbf{r}')/\rho(\mathbf{r}')$ which in 1D reduces to $\delta(\xi)\delta(z - z')/\rho(z')$. Using standard methods, we calculate G as

$$G(z, z', \xi) = \frac{\Theta(\xi)}{2}\operatorname{erfc}\left(\frac{z + z' - \xi}{\sqrt{4\xi}}\right) + \frac{\Theta(\xi)}{\sqrt{4\pi\xi}}\left\{\exp\left[-\frac{(z + z' - \xi)^2}{4\xi}\right] + e^{z'}\exp\left[-\frac{(z - z' - \xi)^2}{4\xi}\right]\right\}, \tag{B2}$$

and G_0, with control "surface" at $z = 0$, as

$$G_0(z, z', \xi) = \frac{\Theta(\xi)}{\sqrt{4\pi\xi}}\left\{e^{z'}\exp\left[-\frac{(z - z' - \xi)^2}{4\xi}\right] - \exp\left[-\frac{(z + z' - \xi)^2}{4\xi}\right]\right\}. \tag{B3}$$

(Both G and G_0 are nondimensionalized by multiplication with $H\rho_0$.) Note that the long-time limits $G_\infty = 1$ and $\lim_{\xi\to\infty} G_0 = 0$.

The general relationship (13) between the boundary propagator G' and G_0 becomes

$$G'(z, \xi) = \partial_{z'} G_0(z, z', \xi)\,|_{z'=0}. \tag{B4}$$

From (B3) and (B4) G', which in 1D is also the transit time pdf $\mathcal{G}'$, follows as

$$G'(z, \xi) = \mathcal{G}'(z, \xi) = \Theta(\xi)\frac{z}{\xi\sqrt{4\pi\xi}}\exp\left[-\frac{(z - \xi)^2}{4\xi}\right], \tag{B5}$$

which is the nondimensional form of $\mathcal{G}'$ as given by HP94 [G' is nondimensionalized through $(H^2/\kappa)G' \to G'$]. We may rewrite (B4) as $G'(z, \xi) = \lim_{z'\to 0} G_0(z, z', \xi)/z'$, which is the 1D-model version of (15).

The probability, $M = \int_0^\infty dz\, e^{-z} G(z, z', \xi) = 1$, while $M_0 = \int_0^\infty dz\, e^{-z} G_0(z, z', \xi)$ is given by

$$M_0(z', \xi) = M_0^\dagger(z', -\xi) = \frac{\Theta(\xi)}{2}\left[\operatorname{erfc}\left(\frac{\xi - z'}{\sqrt{4\xi}}\right) - e^{z'}\operatorname{erfc}\left(\frac{\xi + z'}{\sqrt{4\xi}}\right)\right], \tag{B6}$$

from which (14), $\mathcal{G}'(z, \xi) = -\partial_\xi M_0^\dagger(z, -\xi)$, is readily verified. The population particle-age pdf, $P(\xi)$, is given by

$$P(\xi) = M'(\xi)/M_A = \Theta(\xi)\left[\frac{e^{-\xi/4}}{\sqrt{\pi\xi}} - \frac{1}{2}\operatorname{erfc}\left(\frac{\sqrt{\xi}}{2}\right)\right], \tag{B7}$$

where $M_A = 1$, here. Note the singularity $P(\xi) \to 1/\sqrt{\pi\xi}$ as $\xi \to 0^+$, but that $\int_0^\infty d\xi\, P(\xi) = 1$ and $\langle\xi\rangle \equiv \int_0^\infty d\xi\, \xi P(\xi) = 1$. Thus, the most probable "particle age" of a surface-marked particle is $\xi = 0$, while its expected particle age is $\langle\xi\rangle = 1$.

APPENDIX C

Transit-Time Pdf and Mean Transit Times in Two and Three Dimensions

a. Unbounded domain with radial symmetry in three dimensions

Consider isotropic diffusion without advection in an infinite, unbounded domain of constant density. We impose zero-mixing-ratio BCs over a small spherical bubble of radius $r = a$ centered at the origin of a spherical coordinate system. For simplicity we assume spherical symmetry, so that G_0 is the response to a unit-mass injection distributed over a shell of radius $r = r'$. The nondimensionalized diffusion equation for G_0 can then be written as

$$\left(\partial_t - \frac{\partial^2}{\partial r^2}\right)[rG_0(r, r', t - t')] = \frac{1}{4\pi r}\delta(r - r')\delta(t - t'), \tag{C1}$$

with the BC $G_0(a, r', t - t') = 0$, which has solution

$$G_0(r, r', \xi) = \frac{\Theta(\xi)}{4\pi r r'\sqrt{4\pi\xi}}\left\{\exp\left[-\frac{(r - r')^2}{4\xi}\right] - \exp\left[-\frac{(r + r' - 2a)^2}{4\xi}\right]\right\}. \tag{C2}$$

The bubble-surface-integrated boundary propagator follows from (13) as

$$\mathcal{G}'(r, \xi) = 4\pi a^2 \partial_{r'} G_0(r, r', \xi)|_{r'=a} = \Theta(\xi)\frac{a}{r}\frac{(r - a)}{\xi\sqrt{4\pi\xi}}\exp\left[-\frac{(r - a)^2}{4\xi}\right]. \tag{C3}$$

Equation (C3) also follows from (14) as $\mathcal{G}'(r, \xi) = -\partial_\xi \int_a^\infty dr'\, 4\pi r'^2 G_0(r, r', \xi)$. This quantity has the interpretation of the flux from a unit injection over a shell at r into the bubble at $r = a$. The total amount of mass entering the bubble is

$$\int_0^\infty d\xi\, \mathcal{G}'(r, \xi) = \frac{a}{r}, \tag{C4}$$

which is never unity here because the unboundedness of the domain allows mass to escape to $r = \infty$. Since the time-normalized flux into the bubble still has the natural interpretation of an arrival-time pdf (for pure diffusion, the adjoint problem with time running backward is the same as the direct problem with time running forward), the appropriate transit-time pdf for this problem is not $\mathcal{G}'(r, t)$ but $(r/a)\,\mathcal{G}'(r, t)$. The limit $\lim_{a\to 0}(r/a)\,\mathcal{G}'(r, t)$ is well defined, even though the fraction of tracer mass reaching the infinitesimal bubble goes to zero. Note, however, that independently of the value of a, the mean transit time, $\Gamma \equiv \int_0^\infty d\xi\, \xi\mathcal{G}'(r, \xi)$, is infinite in this setting, due to the fact that particles

can take arbitrarily long paths away from the boundary to give $\mathcal{G}'$ divergent tails.

b. *Mean transit times for a bounded domain with radial symmetry in two and three dimensions*

Here we consider diffusion with constant diffusivity, κ, and constant density in a domain of radial symmetry bounded by inner and outer radii, so that $a \le r \le b$. Over the surface, $r = a$, a δ-function BC is applied on the mixing ratio to obtain $\mathcal{G}'$, and at $r = b$ a zero-flux BC is enforced. In both two and three dimensions (2D and 3D), it is straightforward to obtain the Laplace transform of $\mathcal{G}'$, but we did not obtain a closed-form expression for the inverse transform. Moments (in time) of $\mathcal{G}'(r, t)$ are easily obtained from its Laplace transform, $\tilde{\mathcal{G}}'(r, s)$, since for integer n, we have $\int_0^\infty d\xi\, \xi^n \mathcal{G}'(r, \xi) = (-1)^n \lim_{s\to 0} \partial^n \tilde{\mathcal{G}}'(r, s)/\partial s^n$. For the bounded domain the normalization $\int_0^\infty d\xi\, \mathcal{G}'(r, \xi) = 1$ is confirmed and the mean transit time, Γ, is given in 3D by

$$\Gamma_{3D} = \frac{b^2}{3\kappa}\left[\left(\frac{b}{a} - \frac{b}{r}\right) + \frac{a^2 - r^2}{2b^2}\right], \tag{C5}$$

and in 2D by

$$\Gamma_{2D} = \frac{b^2}{2\kappa}\left[\log\left(\frac{r}{a}\right) + \frac{a^2 - r^2}{2b^2}\right]. \tag{C6}$$

Note that for finite b, Γ is finite for finite a, but diverges like $1/a$ in 3D and like $\log(a)$ in 2D. Similarly, the nth moments $\int_0^\infty d\xi\, \xi^n \mathcal{G}'(r, \xi)$ and $\int_0^\infty d\xi\, (\xi - \Gamma)^n \mathcal{G}'(r, \xi)$ diverge like $1/a^n$ in 3D and like $[\log(a)]^n$ in 2D.

Further insight into the nature of the divergence of Γ as $a \to 0$ is afforded by the correspondence (35) discussed in section 5 between the differential tracer age resulting from a constant source, $\Delta A \propto \chi^+$, and Γ. Consider, for simplicity, the case of advection in the presence of isotropic diffusion (κ), when the time-averaged equation for $\chi^+ = \chi - \chi_0$ may be written as

$$\overline{\mathcal{T}(\chi^+)} = \boldsymbol{\nabla} \cdot (\overline{\mathbf{v}\chi^+}) - \kappa\nabla^2\overline{\chi^+} = \overline{S} - \overline{\partial_t \chi_0}, \tag{C7}$$

where $\partial_t \chi_0$ is the spatially uniform growth rate of the background mixing ratio, and the overbar denotes time average. On sufficiently small spatial scales the diffusion term (highest-order derivative) dominates over advection, so that in the immediate vicinity of a constant point source, $\overline{S} = s_0 \delta(\mathbf{r} - \mathbf{r}_0)$, mixing ratio is determined by $\nabla^2\overline{\chi^+} \propto -\delta(\mathbf{r} - \mathbf{r}_0)$. This means that as the patch radius, $a \to 0$, χ^+, and hence ΔA, diverge in three dimensions like $1/a$, and in two dimensions like $\log(a)$. These are precisely the limiting dependencies of Γ calculated above for the specific purely diffusive models. (An example of a more general two-dimensional case is a zonally averaged model with a point source, corresponding to a line source along a circle of constant latitude.)

REFERENCES

Andrews, A. E., K. A. Boering, B. C. Daube, S. C. Wofsy, E. J. Hintsa, E. M. Weinstock, and T. P. Bui, 1999: Empirical age spectra for the lower tropical stratosphere from in situ observations of CO_2: Implications for stratospheric transport. *J. Geophys. Res.* **104,** 26 581–26 595.

Beining, P., and W. Roether, 1996: Temporal evolution of CFC 11 and CFC 12 concentrations in the ocean interior. *J. Geophys. Res.,* **101,** 16 455–16 464.

Bischof, W., R. Borchers, P. Fabian, and B. C. Kruger, 1985: Increased concentration and vertical distribution of carbon dioxide in the stratosphere. *Nature,* **316,** 708–710.

Boering, K. A., S. C. Wofsy, B. C. Daube, H. R. Schneider, M. Loewenstein, and J. R. Podolske, 1996: Stratospheric mean ages and transport rates derived from observations of CO_2 and N_2O. *Science,* **274,** 1340–1343.

Broeker, W. S., M. Andree, G. Bonani, W. Wolfli, H. Oeschger, M. Klas, A. Mix, and W. Curry, 1988: Preliminary estimates for the radiocarbon age of deep water in the glacial ocean. *Paleoceanography,* **3,** 659–669.

Butkov, E., 1968: *Mathematical Physics.* Addison-Wesley, 735 pp.

Elkins, J. W., and Coauthors, 1996: Airborne gas chromatograph for in situ measurements of long-lived species in the upper troposphere and lower stratosphere. *Geophys. Res. Lett.,* **23,** 347–350.

England, M. H., 1995: The age of water and ventilation time-scales in a global ocean model. *J. Phys. Oceanogr.,* **25,** 2756–2777.

Geller, L. S., J. W. Elkins, J. M. Lobert, A. D. Clarke, D. F. Hurst, J. H. Butler, and R. C. Myers, 1997: Tropospheric SF_6: Observed latitudinal distribution and trends, derived emissions and interhemispheric exchange time. *Geophys. Res. Lett.,* **24,** 675–678.

Haine, T. W. N., and K. J. Richards, 1995: The influence of the seasonal mixed layer on oceanic uptake of CFCs. *J. Geophys. Res.,* **100,** 10 727–10 744.

Hall, T. M., and R. A. Plumb, 1994: Age as a diagnostic of stratospheric transport. *J. Geophys. Res.,* **99,** 1059–1070.

——, and M. J. Prather, 1995: Seasonal evolutions of N_2O, O_2, and CO_2: Three-dimensional simulations of stratospheric correlations. *J. Geophys. Res.,* **100,** 16 699–16 720.

Holzer, M., 1999: Analysis of passive tracer transport as modeled by an atmospheric general circulation model. *J. Climate,* **12,** 1659–1684.

Jenkins, W. J., 1987: ^{3}H and ^{3}He in the beta triangle: Observations of gyre ventilation and oxygen utilization rates. *J. Phys. Oceanogr.,* **17,** 763–783.

Kida, H., 1983: General circulation of air parcels and transport characteristics derived from a hemispheric GCM. Part 2: Very long-term motions of air parcels in the troposphere and stratosphere. *J. Meteor. Soc. Japan,* **61,** 510–522.

Luo, M., R. J. Cicerone, J. M. Russell III, and T. Y. W. Huang, 1994: Observations of stratospheric hydrogen fluoride by Halogen Occultation Experiment (HALOE). *J. Geophys. Res.,* **99,** 16 691–16 705.

Maiss, M., L. P. Steele, R. J. Francey, P. J. Fraser, R. L. Langenfelds, N. B. A. Trivett, and I. Levin, 1996: Sulfur hexafluoride—A powerful new atmospheric tracer. *Atmos. Environ.,* **30,** 1621–1629.

McFarlane, N. A., G. J. Boer, J.-P. Blanchet, and M. Lazare, 1992: The Canadian Climate Centre second generation general circulation model and its equilibrium climate. *J. Climate,* **5,** 1013–1044.

Morse, P. M., and H. Feshbach, 1953: *Methods of Theoretical Physics.* McGraw-Hill, 997 pp.

Mote, P. W., T. J. Dunkerton, M. E. McIntyre, E. A. Ray, and P. H. Haynes, 1998: Vertical velocity, vertical diffusion, and dilution by midlatitude air in the tropical lower stratosphere. *J. Geophys. Res.,* **103,** 8651–8666.

Plumb, R. A., and D. D. McConalogue, 1988: On the meridional structure of long-lived tropospheric constituents. *J. Geophys. Res.,* **93,** 15 897–15 913.

Prather, M. J., 1986: Numerical advection by conservation of second order moments. *J. Geophys. Res.,* **91,** 6671–6681.

——, M. B. McElroy, S. C. Wofsy, G. Russell, and D. Rind, 1987: Chemistry of the global troposphere: Fluorocarbons as tracers of air motion. *J. Geophys. Res.,* **92,** 6579–6613.

Rind, D., R. Suozzo, N. K. Balachandran, A. Lacis, and G. Russell, 1988: The GISS global climate/middle atmosphere model. Part I: Model structure and climatology. *J. Atmos. Sci.,* **45,** 329–370.

Shraiman, B. I., and E. D. Siggia, 1994: Lagrangian path integrals and fluctuations in random flows. *Phys. Rev. E,* **49,** 2912–2927.

Zabel, R. W., and J. J. Anderson, 1997: A model of the travel time of migrating juvenile salmon, with an application to Snake River spring chinook salmon. *North Amer. J. Fish. Manage.,* **17,** 93–100.